

# A plethora of new R Coronae Borealis stars discovered from a dedicated spectroscopic follow-up survey<sup>★</sup>

P. Tisserand<sup>1,2</sup>, G. C. Clayton<sup>3</sup>, M. S. Bessell<sup>2</sup>, D. L. Welch<sup>4</sup>, D. Kamath<sup>2,6</sup>, P. R. Wood<sup>2</sup>, P. Wils<sup>5</sup>,  
Ł. Wyrzykowski<sup>7</sup>, P. Mróz<sup>7</sup>, and A. Udalski<sup>7</sup>

<sup>1</sup> Sorbonne Universités, UPMC Univ. Paris 6 et CNRS, UMR 7095, Institut d’Astrophysique de Paris, IAP, 75014 Paris, France  
e-mail: [tisserand@iap.fr](mailto:tisserand@iap.fr)

<sup>2</sup> Research School of Astronomy and Astrophysics, Australian National University, Cotter Rd, Weston Creek ACT 2611, Australia

<sup>3</sup> Department of Physics & Astronomy, Louisiana State University, Baton Rouge, LA 70803, USA

<sup>4</sup> Department of Physics & Astronomy, McMaster University, Hamilton, Ontario L8S 4M1, Canada

<sup>5</sup> Vereniging Voor Sterrenkunde (VVS), Brugge, Belgium

<sup>6</sup> Department of Physics and Astronomy, Macquarie University, Sydney, NSW 2109, Australia

<sup>7</sup> Astronomical Observatory, University of Warsaw, Al. Ujazdowskie 4, 00-478 Warszawa, Poland

Received 10 October 2018 / Accepted 11 December 2019

## ABSTRACT

**Context.** It is more and more suspected that R Coronae Borealis (RCB) stars – rare hydrogen-deficient and carbon-rich supergiant stars – are the products of mergers of CO/He white-dwarf binary systems in the intermediate mass regime ( $0.6 < M_{\text{Tot}} < 1.2 M_{\odot}$ ). Following the merger, a short-lived cool supergiant phase starts. RCB stars are extremely rare as only 77 have hitherto been known in the Galaxy, while up to 1000 have been predicted from population synthesis models.

**Aims.** The goal is to significantly increase the number of known RCB stars in order to better understand their evolutionary paths, their spatial distribution, and their formation rate in the context of population synthesis results. A list of 2356 RCB star candidates was selected using infrared colours from the all-sky 2MASS and WISE surveys. The objective is to follow them up spectroscopically to classify the candidates and, thus, to distinguish RCB stars from other dust-producing stars.

**Methods.** A series of brightness and colour-colour cuts that were used as selection criteria were then tested using the sample of known Galactic and Magellanic RCB stars. RCB spectral energy distribution models were also used to understand the effects of each selection criterion in terms of circumstellar shell temperature. Optical, low-resolution spectra were obtained for nearly 500 of the candidate stars. These spectra were compared to synthetic spectra from a new grid of MARCs hydrogen-deficient atmospheric models. This allowed us to define a spectroscopic classification system for RCB stars depending on their effective temperature and photometric status.

**Results.** This programme has found 45 new RCB stars, including 30 Cold ( $4000 < T_{\text{eff}} < 6800$  K), 14 Warm ( $6800 < T_{\text{eff}} < 8500$  K), and one Hot ( $T_{\text{eff}} > 15000$  K). Forty of these belong to the Milky Way and five are located in the Magellanic Clouds. We also confirmed that the candidate KDM 5651 is indeed a new RCB star, increasing the total number of Magellanic RCB stars to 30.

**Conclusions.** We increased the total number of RCB stars known by ~50%, bringing it up to 147. In addition, we compiled a list of 14 strong RCB candidates, most certainly observed during a dust obscuring phase. From the detection efficiency and success rate so far, we estimate that there should be no more than 500 RCB stars existing in the Milky Way, all HdC stars included.

**Key words.** methods: observational – stars: carbon – stars: chemically peculiar – supergiants – stars: evolution

## 1. Introduction

R Coronae Borealis (RCB) stars are rare hydrogen-deficient, carbon-rich, supergiant stars that are increasingly suspected of having resulted from the merger of one CO- + one He- white dwarfs (Clayton 2012). Therefore, they may be low-mass analogues of Type Ia supernova progenitors. The double-degenerate scenario has been strongly supported by the observations of abundance anomalies in RCB stars including a large  $^{18}\text{O}$  overabundance in their atmospheres (Clayton et al. 2007; García-Hernández et al. 2010) and of surface abundance anomalies for a few elements, fluorine in particular (Pandey et al. 2008; Jeffery et al. 2011). Furthermore, the abundances computed by

simulations of such merging events agree well with the peculiar and disparate atmosphere abundances observed in RCB stars (Jeffery et al. 2011; Staff et al. 2012; Menon et al. 2013; Zhang et al. 2014; Lauer et al. 2019).

Interestingly, a second evolutionary scenario, the final helium shell flash, has also been proposed to explain the origin of RCB stars (Iben et al. 1996; Renzini 1990). The final-flash in a star on the verge of becoming a WD, causes it to expand into a cool supergiant star similar to RCB stars. Therefore, a fraction of RCB stars may result from the final-flash scenario. Such objects could be identified from the detection of hydrogen-rich nebulae around them (Clayton et al. 2011). However, recent studies of some RCB’s immediate circumstellar environment do not favour that scenario (Montiel et al. 2015, 2018).

Our goal is to test these two scenarios by increasing the numbers of known RCB stars and consequently studying their sky distribution and formation rate. In the double-degenerate

<sup>★</sup> Full Table 2 and the spectra presented in Figs. 5, 6, 9, 11, and 13 are only available at the CDS via anonymous ftp to [cdsarc.u-strasbg.fr](ftp://cdsarc.u-strasbg.fr) (130.79.128.5) or via <http://cdsarc.u-strasbg.fr/viz-bin/cat/J/A+A/635/A14>

scenario, it is estimated that the He-CO WDs merger birthrate should be between  $\sim 10^{-3}$  and  $\sim 5 \times 10^{-3}$  per year (Nelemans et al. 2001; Ruiter et al. 2009; Karakas et al. 2015) and that an RCB phase lifetime should last about  $10^5$  years, as predicted by theoretical evolution models (Saio & Jeffery 2002). Therefore, we can expect between 100 and 500 RCB stars to exist in our Galaxy.

RCB stars possess a large range of photospheric temperatures, mostly between  $\sim 4000$  and  $8000$  K (Tisserand et al. 2009; Tisserand 2012), but some are also known at hotter temperature ( $> 12000$  K) (De Marco et al. 2002). This wide range of effective temperatures supports the scenario that after the cataclysmic event that creates an RCB, it goes through a supergiant phase which then evolves from a cold to a warm state while the helium-rich atmosphere contracts (Jeffery et al. 2011; Lauer et al. 2019). Fortunately, RCB stars are also known to be very bright,  $-5 \leq M_V \leq -3.5$  (Tisserand et al. 2009, Fig. 3). All RCB stars have an IR excess due to the presence of a warm circumstellar dust shell with  $300 < T_{\text{eff,shell}} < 1000$  K (Tisserand 2012, Fig. 2). These two characteristics facilitate the search reported here using the ensemble of photometric datasets available. Finally, we note that RCB stars are members of a larger class of stars called the Hydrogen deficient Carbon stars (HdC stars) that share similar spectroscopic characteristics, but RCB stars have the particularity of being surrounded by dust and of undergoing unpredictable fast and large photometric declines due to clouds of dust newly produced.

We search for new RCB stars located in the Milky Way and the Magellanic Clouds in two steps: firstly, by selecting a short-list of targets of interest (ToI) among the 500 million objects catalogued within the two all-sky near- and mid-infrared (IR) surveys, 2MASS (Skrutskie et al. 2006) and WISE (Wright et al. 2010); secondly, by following them up spectroscopically, possibly with added support from photometric monitoring surveys.

Section 2 presents the WISE survey and describes the broad-band, colour selection criteria applied to the 2MASS and WISE ALL-Sky catalogues. The resulting list of RCB star candidates, their characteristics and the subsequent classification into priority groups for the spectroscopic follow-up are discussed in Sects. 2.4 and 2.5. Then in Sect. 3, we detail the new spectra obtained, the light curves, and the stellar atmosphere models used. The spectral analysis and the classification system developed to identify new RCB stars are discussed in Sect. 4, while the status of previously discovered RCB candidates is reviewed in Sect. 5. In Sect. 6, we explore the RCB star spatial distribution, and estimate the total number of RCB stars in the Milky Way. Finally, we summarise our results in Sect. 7.

## 2. Infra-red broad bands selection of targets of interest

### 2.1. WISE All-Sky catalogue and Known RCB stars

The WISE Explorer mapped in 2010, during its full cryogenic phase, the entire sky in 3.4, 4.6, 12 and  $22 \mu\text{m}$  with, respectively, angular resolutions of 6.1, 6.4, 6.5 and  $12.0 \text{ arcsec}$  and 0.08, 0.11, 1.0 and  $6.0 \text{ mJy}$  in point source sensitivities at 5 sigma (Wright et al. 2010). The four WISE photometric bands are hereafter named [3.4], [4.6], [12] and [22]. There was a Preliminary Data release in 2011 (WISE-PDR1) covering 57% of the full sky area (Cutri et al. 2011), and the All-Sky Data Release (WISE All-Sky) containing more than 563 million objects in 2012 (Cutri et al. 2012).

We chose to use the WISE All-Sky catalogue instead of the latest release, the ALLWISE catalogue (Mainzer et al. 2011),

which was made after combining the data obtained during the cryogenic and post-cryogenic survey (NEOWISE) phases, for the following reasons. Firstly, it is preferable when selecting objects as highly variable as RCB stars to compare magnitudes taken at the same epoch (photometric variations as large as  $\sim 0.5 \text{ mag}$  can be observed at 3 microns). Secondly, the ALLWISE combined dataset observations were made at different temperature states of the spacecraft and the [3.4] and [4.6] photometric sensitivities changed following the depletion of the solid hydrogen cryogen and subsequent warm-up of the detectors (see the Data Release Explanatory Supplement for more information). Therefore the photometric bias observed for saturated sources has also changed and is therefore not uniform for all measurements listed in ALLWISE. This is important as the majority of known Galactic RCB stars are saturated in the [3.4] and [4.6] photometric bands. A correction of these biases would be complicated to apply on the entire ALLWISE dataset, instead we found a pragmatic solution with the entire WISE All-Sky catalogue as its dataset can be considered as homogeneous. Finally, RCB stars are bright objects (all known RCB stars are brighter than 9 mag in [12] – see histogram in Fig. 1, top-right) and, with a magnitude limit of  $\sim 13 \text{ mag}$  in [12], the WISE All-Sky catalogue is sufficient for our search. A deeper dataset like ALLWISE would not improve it. The magnitude limit offered by the WISE All-Sky catalogue allow us to detect Galactic and Magellanic RCB stars within about 50 kpc in all four mid-infrared bands.

From the WISE-PDR1 catalogue, a preliminary list of candidate RCB stars was created (Tisserand 2012) using selection criteria based on the peculiar near- and mid-infrared colours of RCB stars and their circumstellar dust. This first list is now superseded by the sample selected here using the WISE All-Sky catalogue. The new catalogue is much improved in the sky coverage and the photometric sensitivity. In addition, the Magellanic Clouds are now included in the catalogue. Furthermore, the WISE All-Sky detection algorithm, used in a highly crowded field, is more efficient. Consequently, some known RCB stars such as OGLE-GC-RCB-1 & -2, that were not catalogued in the WISE-PDR1 despite being clearly bright, are now listed in the WISE All-Sky catalogue.

All 101 known RCB stars (77 of those are Galactic and 24 are Magellanic) have been catalogued in the WISE All-Sky release, as well as ten stars that are considered as strong RCB candidates (Clayton 2012; Tisserand et al. 2013). The WISE magnitudes and associated  $1\sigma$  uncertainties are listed in Table A.1. This list of known RCB stars has been used as a benchmark in our search for new members of the class. An update on the status of the ten strong RCB star candidates is given in Sect. 5 after the analysis of their broad-band IR photometry and of the newly available spectra.

We found small photometric zero-point shifts between the two WISE catalogues: All-Sky – PDR1  $\sim -13 \text{ mmags}$  [3.4],  $\sim -4 \text{ mmags}$  [4.6],  $\sim 29 \text{ mmags}$  [12], and  $\sim -27 \text{ mmags}$  [22]. These differences are small but could have a significant impact on the selection thresholds already defined in Tisserand (2012) if not taken into account (see Sect. 4).

Most known Galactic RCB stars are highly saturated in the [3.4] and [4.6] bands. Fortunately, photometry was nevertheless performed by fitting only the PSF wings. However, particularly in the [4.6] band, this resulted in a photometric bias for all objects brighter than about  $[4.6] < 6.5 \text{ mag}$  (see Sect. III.3.c of WISE All-Sky Release Explanatory Supplement for more information). For the brightest objects, the [4.6] magnitude could be over-estimated by almost 1 magnitude. To correct for this effect,

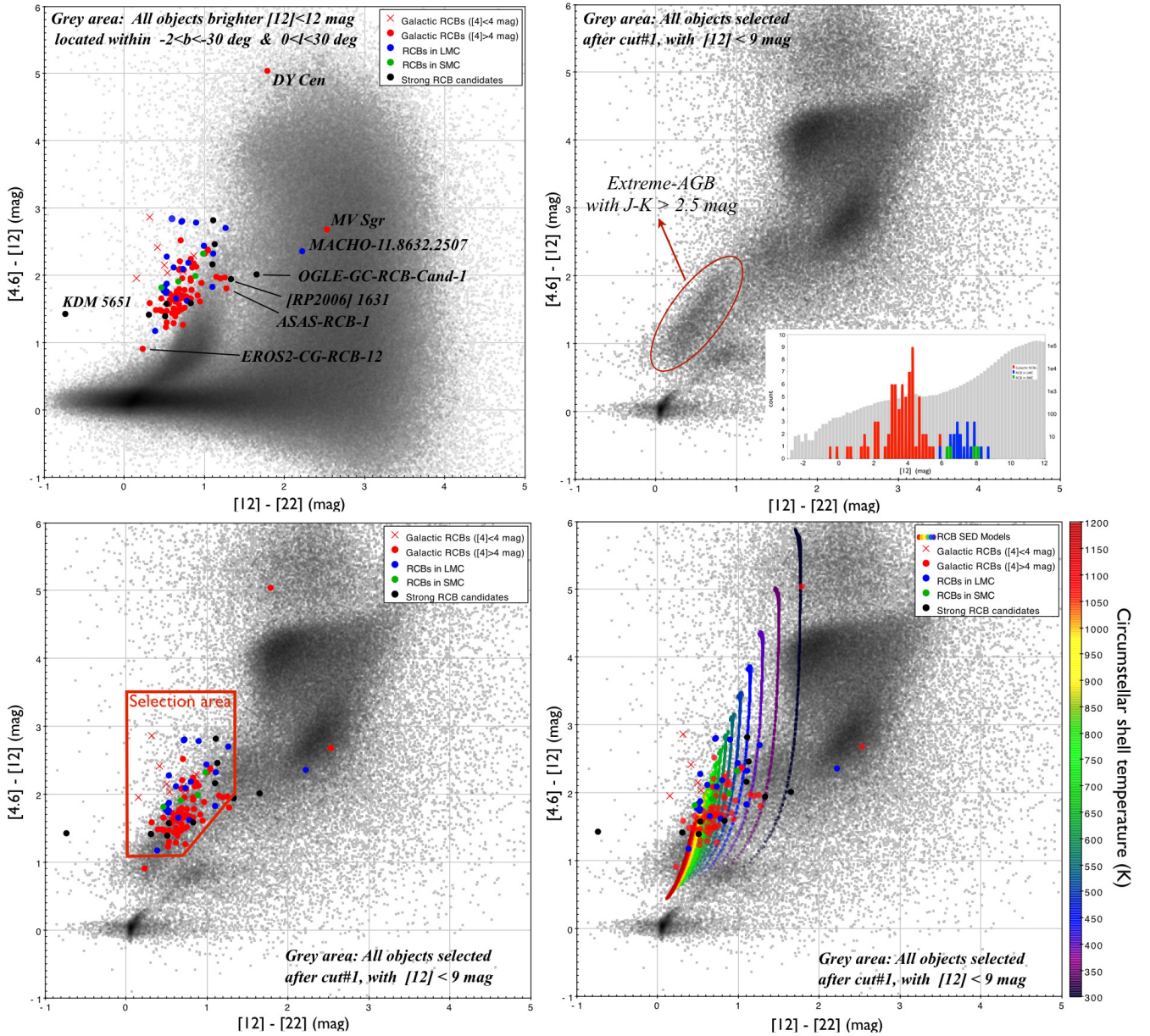


**Fig. 1.** Four panels representing the same colour–colour  $[4.6] - [12]$  versus  $[12] - [22]$  diagram for different WISE source subsamples. See the explanations in the text and within the figures. The  $[12]$  magnitude distribution represented inside the *top-right panel* corresponds to the known RCB stars (linear scale, coloured bins: red for Galactic, blue for LMC, green for SMC) and to the WISE objects selected after cut #0 (grey bins, logarithmic scale). The names and positions of all known and candidate RCB stars that were rejected by the criterion cut #2 are indicated on the *top-left panel*.

we used the same strategy as the one detailed in Tisserand (2012, Sect. 2.2.1). A corrected  $[4.6]_{\text{corr}}$  magnitude was estimated from the spectral energy distributions (SEDs) of known RCB stars. We derived the following linear correction formula for the WISE All-Sky dataset:  $[4.6]_{\text{corr}} = 0.83 \times [4.6]_{\text{cat}} + 1.09$ . We applied this correction to all objects brighter than  $[4.6]_{\text{cat}} < 6.35$  mag. For the brightest objects,  $[4.6]_{\text{cat}} < 4$  mag, we assume that we do not know the brightness better than 10% and modified the respective WISE errors.

## 2.2. Selection criteria

RCB stars are so rare and so diverse in terms of photospheric and circumstellar-shell luminosities and temperatures that to obtain a comprehensive view over the entire range of these

parameters, we decided to cast a wide net over the entire 2MASS (Skrutskie et al. 2006) and WISE (Wright et al. 2010) databases. The association between these two catalogues is already provided by the IR science archive (IRSA) from NASA. Firstly, the main selection criteria were applied to all catalogued objects that presented valid measurements in all seven (3 2MASS + 4 WISE) bands (Sect. 2.2.1). Subsequently, to catch RCB stars observed in a faint phases, new criteria are defined for a large number of detected objects that are listed with some upper limits values in up to two of these seven bands (Sect. 2.2.2).

To simplify our search in these two cases, we required at the start of our analysis that each object should be detected in the WISE  $[12]$  band and be brighter than  $[12] < 12$  mag. That corresponds to  $\sim 21.5$  and  $\sim 33.2$  million objects respectively for the first and second group, which overall correspond to nearly

**Table 1.** Number of selected Galactic (G) and Magellanic (M) objects remaining after each selection criterion.

Selection criterion	Number of objects reported with 7 valid measurements	Number of objects reported with at least one upper limit value in $J, H, K, [3]$ or $[22]$	Number of known RCB stars selected	Known RCB stars eliminated at each stage
0: $[12] < 12$ mag	21532159	33203403	100	V1157 Sgr
1: Cut on ( $J - H$ vs. $H - K$ )	1843558	1582645	95	ASAS-RCB-8, XX Cam, Y Mus, UV Cas and EROS2-LMC-RCB-6
2: Cut on ( $[4.6] - [12]$ vs. $[12] - [22]$ )	14315	243710	90	ASAS-RCB-1, DY Cen, EROS2-CG-RCB-12, MV Sgr and MACHO-11.8632.2507
3: Cut on ( $J - K$ vs. $J - [12]$ )	G: 11301, M: 482	232899	89	MACHO-308.38099.66
4: Cut on ( $[12]$ vs. $[12] - [22]$ )	G: 2568, M: 255	4279		
5: Cut on ( $K$ vs. $J - K$ )	G: 2024, M: 118	4204		
6: Cut on ( $[3.4] - [4.6]$ )	G: 1905, M: 112	2435		
7: Cut on 2MASS-WISE Association	G: 1862, M: 109	1736		
Special supplementary cuts targeting objects with upper limit values in the $J$ and/or $[22]$ bands				
8: Outside $ b  < 2$ , $ l  < 60$ deg		757	88	EROS2-CG-RCB-8
9: Strict cuts on blending		473	87	EROS2-CG-RCB-5
Final, without known RCB stars and the known HdC star HD 175893	G: 2194, M: 162			

10% of the 563 million objects detected in the WISE All-Sky survey. The  $[12]$  threshold was chosen to be conservative as it is fainter than the faintest known Magellanic RCB stars by three magnitudes (see the  $[12]$  distribution in Fig. 1, top-left). Using all known RCB stars, it is worth mentioning also that the median of the signal-to-noise ratio distribution in  $[12]$  is higher by a factor of two than those for the three remaining WISE bands. RCB stars are therefore most noticeable in the  $[12]$  bandpass.

For the definition of our selection criteria, we used all 102 known RCB stars as benchmarks, as well as comparing to RCB SED models with a range of photospheric (4000–8000 K) and circumstellar-shell temperatures (300–1200 K). The summary of the selection criteria applied, the resulting number of candidate stars selected, and the known RCB stars rejected are presented in Table 1.

### 2.2.1. The main selection criteria

**Cut 0.** We kept all objects that were detected with a valid measurement in each of the seven 2MASS+WISE bands, and were found to be brighter than  $[12] < 12$  mag. Only three known RCB stars did not pass these simple requirements. V1157 Sgr was not selected because it was not detected in both  $[12]$  and  $[22]$  as it is located in a part of the sky with no observational coverage in these two bandpasses. MSX-SMC-014 and EROS2-CG-RCB-8 had two upper limit values in 2MASS  $J$  and  $H$ . However, these two RCB stars will still be considered in the second selection scenario applied to objects that possess upper limit values (see Sect. 2.2.2).

**Cut 1.** The first colour–colour selection criterion was applied on the  $J - H$  versus  $H - K$  diagram. It targets objects presenting a high near-infrared excess as RCB stars possess warm circumstellar shells. This selection criterion has already proved its high efficiency in previous studies (Tisserand 2012, Fig. 6) and remains the same. It was defined as a function of the Galactic latitude as

the interstellar extinction affects these infrared magnitudes significantly. We have now rejected  $\sim 91\%$  of all previously selected objects at this stage. However, four known RCB stars were also rejected: ASAS-RCB-8, XX Cam, Y Mus and UV Cas. This is because all of them are warm RCB stars ( $T_{\text{eff}} > 7200$  K) with their respective shells not thick enough to impact on their near-IR magnitudes. Their SEDs are displayed in Tisserand (2012) and Tisserand et al. (2013).

It is important to mention here that the main locus of classical carbon stars (located at  $J - H \sim 0.6$  mag and  $H - K \sim 1.2$  mag) is entirely rejected at this stage.

**Cut 2.** The second colour–colour selection criterion was applied directly to the WISE photometry, and more specifically on the  $[4.6] - [12]$  versus  $[12] - [22]$  diagram. It therefore focuses on RCB dust shell temperatures. A similar criterion was used by Tisserand (2012), but we adjusted the selection thresholds here to better suit the new photometric datasets (i.e. due to the change in photometric zero-point between the preliminary and the All-Sky catalogues, see Sect. 2.1) and the stellar distribution of the new known RCB stars. The selection area is illustrated in Fig. 1 (bottom, left) and the limits are the following:

$$1.1 < [4.6] - [12] < 3.5 \quad \text{and} \quad 0 < [12] - [22] < 1.35 \\ \text{and} \quad [4.6] - [12] \geq 1.5 \times ([12] - [22]) + 0.05 \quad (1)$$

Figure 1 shows four examples of the same  $[4.6] - [12]$  versus  $[12] - [22]$  colour–colour diagram using different object subsamples and with RCB SED models illustrated for different circumstellar dust shell temperatures. First, top-left, the positions of the known RCB stars are indicated as well as a sample of catalogued objects selected after cut #0. This panel shows that most RCB stars form a locus with mid-infrared colours that are uncharacteristic of ordinary catalogued objects. For the remaining three panels, the sample of objects plotted has passed the IR selection cut #1 and, for illustrative purposes only, are brighter than

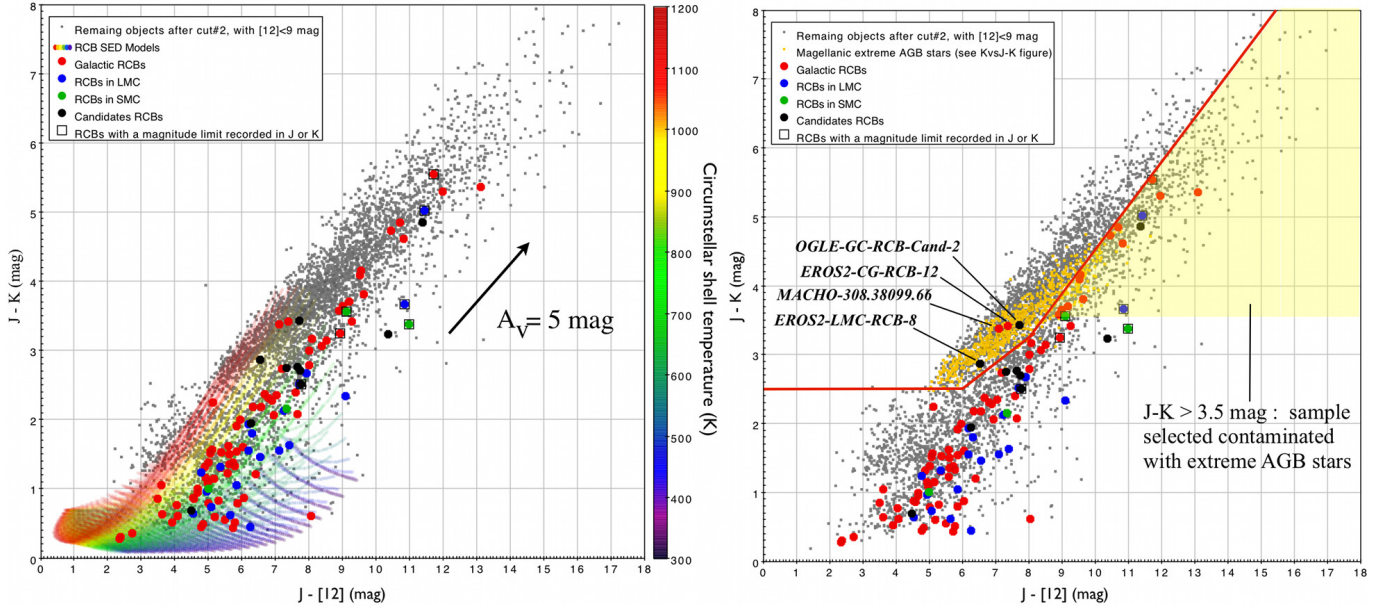


**Fig. 2.**  $J - K$  versus  $J - [12]$  colour–colour diagrams with all objects selected after cut #2 and brighter than  $[12] < 9$  mag, and with all known and candidate RCB stars represented. On the *left side*, RCB SED models are overlaid with a colour scale related to the circumstellar shell temperature. The interstellar extinction arrow is also indicated, it shows that many RCB stars were indeed affected by extinction at the time of the 2MASS epochs. This extinction includes circumstellar and interstellar dust. RCB stars observed in a deep decline have their 2MASS  $J$  magnitudes recorded with a magnitude limit. On the *right side*, the Magellanic extreme-AGB stars are represented with orange dots (see Fig. 3). The selection area of cut #3 is delimited with red lines. Four known or candidate RCB stars that were not selected are marked with their names. This plot shows that all selected objects redder than  $J - K > 3.5$  mag will be contaminated by extreme AGB stars. RCB stars will also be even harder to find with such high extinction.

$[12] < 9$  mag, which is a magnitude corresponding more closely to our reference sample of known RCB stars (see, within the top-right graph, the  $[12]$  mag distribution for the known RCB stars and for the selected WISE objects after cut #1). An elongated feature appears near the RCB-star locus, corresponding to highly enshrouded AGB stars with  $J - K > 2.5$  mag. Most of the known Galactic RCB stars are distributed over the redder part of that feature, while the Magellanic stars are more dispersed, with more than half lying above this AGB clump ( $[4.6] - [12] > 2$  mag). It could possibly indicate that Magellanic RCB stars have thicker circumstellar dust shells than their Galactic counterparts. More studies will be necessary to understand this difference. We display on the bottom-right panel the theoretical colours of RCB stars estimated from SED models. It shows that our selection criteria cut #2 does not select RCB stars with very cold shell temperatures ( $T_{\text{shell}} < 400$  K) or with hot thin circumstellar shells.

A staggering 99% of objects, that passed the selection cut #1, were rejected by that particular criterion, while five known RCB stars were also not selected (i.e. ASAS-RCB-1, EROS2-CG-RCB-12, DY Cen, MV Sgr and MACHO-11.8632.2507), as well as three RCB candidates (i.e. KDM 5651, OGLE-GC-RCB-Cand-1 and [RP2006] 1631). Four of these eight objects, DY Cen, MV Sgr, MACHO-11.8632.2507 and OGLE-GC-RCB-Cand-1, lie far from the main RCB locus on the  $[4.6] - [12]$  versus  $[12] - [22]$  diagram. For the first three, this is explained by the presence of a second bright cold dust shell around them – Radiative transfer modelling of seven RCB stars with Far-IR data found that all of them have two dust shells (Montiel et al. 2018). ASAS-RCB-1 and the candidate [RP2006] 1631 lie just outside the selection limit as they both have a cold thick shell ( $T_{\text{shell}} \sim 400$  K or colder). On the contrary, EROS2-CG-RCB-12 was eliminated because of its warm thin shell. Finally,

RCB candidate KDM 5651 was found with a negative  $[12] - [22]$  colour, at odds with typical values found for known RCB stars. However, its  $[22]$  magnitude was reported with a very large error of 0.4 mag indicating a large uncertainty on its  $[22]$  brightness. The  $[22]$  measurement reported in the subsequent WISE ALL-WISE catalogue was corrected from this obvious photometric bias, and we found that KDM 5651 would then have passed selection cut #2.

**Cut 3.** This criterion is less efficient than the previous ones, as it rejects only 20% of the remaining sample (after cut #2), but it is valuable as it targets mainly the more common AGB stars. We explain the reason of this selection with the two panels presented in Fig. 2. There, we illustrate the distribution of RCB stars and of the remaining sample in the colour–colour  $J - K$  versus  $J - [12]$  diagram. For a better understanding, one can also look at Fig. 7 presented by Tisserand (2012), where the distributions of objects coloured coded with their respective SIMBAD classification are shown.

In the left-hand panel, the RCB SED models are colour-coded by circumstellar dust shell temperature. One can recognize that not all known RCB stars are located within the area covered by these models. This is the case for about a quarter of them, that have a  $J - K$  colour index higher than about 3 mag. This is due to the combination of interstellar reddening and the characteristic high reddening that occurs when newly formed carbon dust clouds are on the line of sight and therefore obscure suddenly the photosphere. RCB stars that have been observed undergoing such rapid decline events, are found to have the highest  $J - K$  colour index. This is why also the RCB stars with upper limit values in either the  $J$  or  $K$  2MASS bands are all located outside the area covered by the RCB SED models. In the right-hand panel, we added the distribution of Magellanic extreme AGB stars (see cut #5 and Fig. 3 for an explanation of

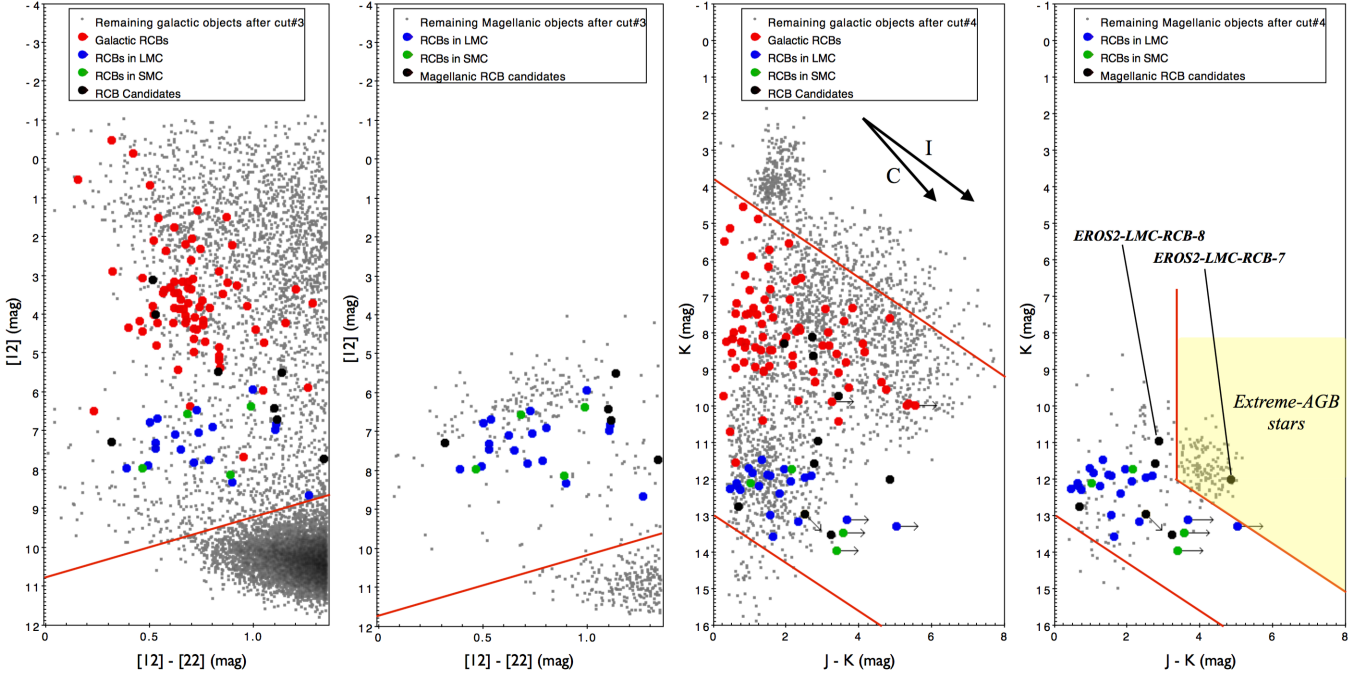


**Fig. 3.** Colour–magnitude diagrams  $[12]$  versus  $[12]-[22]$  and  $K$  versus  $J-K$  for respectively the remaining Galactic and Magellanic objects sample selected after cut #3. The selection areas of cut #4 and cut #5 are delimited with red lines. All known and candidate RCB stars are indicated also as a reference sample. The area where Magellanic extreme AGB stars were selected to be represented in Fig. 2 is indicated in orange. See discussion in Sect. 2.2.1, cut #4 and cut #5 for more details. The interstellar (I) and circumstellar (C) reddening effect are indicated with arrows.

the selection of these extreme AGB stars used here for illustration) as well as the limits of the selection criteria. This selection was designed to remove a high fraction of the extreme AGB stars. However, above a  $J-K$  colour index of 3.5 mag, our sample will still be contaminated by such objects as we designed our cuts to keep also RCB stars reddened by decline events. On the other side of the diagram, our criteria have the negative effect of removing potential RCB stars that possess a warm dust shell ( $T_{\text{shell}} > 900$  K), in the following scenarios: RCB stars with thick shells and, RCB stars observed during a high extinction phase or located near the Galactic plane. This is the reason why two known RCB stars did not pass the selection, namely, MACHO-308.38099.66 and EROS2-CG-RCB-12 (which was already rejected by cut #2). Two RCB candidates, OGLE-GC-RCB-Cand-2 and EROS2-LMC-RCB-8, were also rejected in a similar way. However, the situation here may be different as they are located in the diagram at the expected position of the AGB stars locus, and their respective light curves show unusually large amplitude oscillations for RCB stars. A more detailed discussion on their possible nature is given in Sect. 5. Here are the limits of the selection applied:

$$J-K \leq 2.2 \quad \text{if} \quad (J-[12]) < 6 \quad (2)$$

$$J-K \leq (3.0 \times (J-[12]) - 7.0)/5 \quad \text{if} \quad (J-[12]) \geq 6. \quad (3)$$

**Cut 4.** At this stage, we separate the selected sample into two groups: the objects detected towards the Magellanic Clouds and the Galactic sample. It was a necessary split as the following selection is on apparent magnitude.

The first selection focuses on the shell brightness using the  $[12]$  band as an indicator. The two panels on the left side of Fig. 3 represent the colour–magnitude diagrams  $[12]$  versus  $[12]-[22]$  for both samples. The applied selection criteria are listed below in Eq. (4) and are represented on each panel. They correspond

to faint limits and are used only to remove a group of faint red objects that are almost certainly all galaxies. For the Magellanic sample, we decided to be less restrictive by 1 mag as the number of objects added was small.

These criteria remove about 75% of remaining objects selected after cut #3. None of the known RCB stars were eliminated at that stage.

$$\text{Galactic} : [12] \leq -1.53 \times ([12]-[22]) + 10.76$$

$$\text{Magellanic} : [12] \leq -1.53 \times ([12]-[22]) + 11.76. \quad (4)$$

**Cut 5.** Here we apply a selection cut on the photospheric brightness. We used the  $K$  band as an indicator as it is the photometric band that is the least affected by possible declines due to newly formed dust clouds that obscure the photosphere. The bright and faint limits are shown in the two colour–magnitude diagrams represented on the right side of Fig. 3 and are also listed in Eq. (5) below. For the Magellanic sample, the bright limit was truncated at  $J-K > 3.3$  mag to keep potential interesting Galactic RCB candidates located on the line of sight of the Magellanic Clouds but also to remove a group of extreme AGB stars concentrated in the bright red side of that diagram. About 28% of the remaining objects were rejected at this stage, while keeping all known RCB stars. Only the Magellanic RCB candidate, EROS2-LMC-RCB-7, did not pass these selection criteria being located within the group of extreme AGB stars.

$$\text{Both samples} : K \geq 0.68 \times (J-K) + 4.0$$

$$\text{Galactic} : K \leq 0.68 \times (J-K) + 13.0$$

$$\text{Magellanic} : K \leq 0.68 \times (J-K) + 9.7 \quad \text{if} \quad (J-K) \geq 3.3. \quad (5)$$

**Cut 6.** We apply here a selection using the last unused filter, the [3.4] WISE band. In a colour–colour  $[3.4]-[4.6]$  versus  $[12]-[22]$  diagram, we found that there was a possibility to

clean up a bit more our sample by keeping all objects redder than  $[3.4]-[4.6] > 0.2$  mag. This criterion targets objects that one cannot justify to keep in the final catalogue because they are bluer than the bluer edge of all SED models calculated and of any known RCB stars (see Fig. 4). Only about a hundred objects were eliminated with this criterion.

*Cut 7.* Finally, we studied the distribution of distances between the 2MASS and WISE catalogues (Cutri et al. 2012). The RMS accuracy of the reconstructed WISE positions with respect to 2MASS for unsaturated sources with the signal-to-noise ratio  $>50$  in unconfused regions of the sky is approximately 200 mas on each axis. Our targets are very bright stars located mostly in a crowded environment. We decided to apply no cuts if the stars were brighter than  $[12] < 4$  mag as we observed a wide range of variation for the association distance, however, for fainter objects we requested that the association distance to be lower than one arcsecond. Only 46 objects were rejected.

### 2.2.2. Description of the specific criteria targeting objects listed with upper limits

A majority of the WISE All-Sky objects detected are listed with an upper limit value in at least one of the seven bands (3 2MASS + 4 WISE). This could be due to multiple technical or physical reasons, but nevertheless some of these objects could be potentially interesting. Indeed, we found that 8 of the 101 known RCB stars are reported as such. Four of them are reported with only an upper limit value in the  $J$  band (EROS2-SMC-RCB-1, EROS2-LMC-RCB-6, EROS2-CG-RCB-5 and MACHO-6.6575.13); one with an upper limit in the  $K$  band (ASAS-RCB-20, with a surprising bright  $K$  upper limit value of  $\sim 9.9$  mag); two known RCB stars present upper limits values in the  $J$  and  $H$  bands (MSX-SMC-014 and EROS2-CG-RCB-8); and one known RCB star, V1157 Sgr, with no measurements reported in the WISE  $[12]$  and  $[22]$  bands (see discussion above in cut #0). We are particularly familiar with the game of hide and seek played by RCB stars. The upper limits for 2MASS measurements<sup>1</sup> are in most cases due to observations made during a phase of a large photometric decline (which can go up to  $\sim 3.0$  mags in  $J$  and  $\sim 1.6$  mag in  $K$  during a maximum decline event of  $\Delta \sim 9$  mag observed in  $V$ ). The light curves as well as the 2MASS epochs for each of the known RCB stars, listed above, can be found in Tisserand et al. (2004, 2008, 2009). In the particular case of ASAS-RCB-20, we found that its non-detection in the  $K$  band is due to a confusion between multiple sources that the 2MASS detector algorithm did not succeed in resolving it.

About 33.2 million objects, brighter than  $[12] < 12$  mag and detected in both  $[4.6]$  and  $[12]$  photometric bands, were reported with an upper limit in at least one of the remaining five bands:  $J$ ,  $H$ ,  $K$ ,  $[3.4]$  or  $[22]$ . We concentrated our analysis on these objects. Understandably, for 29 million of them ( $\sim 87\%$ ), the  $[22]$  band was the only one affected. That is the least sensitive of the WISE photometric bands. We studied the 2MASS and WISE datasets more closely to analyse the reality of the situation and confirmed that when only the  $J$  or the  $[22]$  bands are reported with upper limit values, the objects are indeed predominantly

not detected in these bands. However, in the following specific scenarios, when a measurement was only missing in the  $H$  or  $K$  bands, or only in both  $J$  and  $K$  bands, the related objects were in fact usually blended with one or more nearby objects. We have redesigned our selection criteria to suit each of these scenarios. The changes added in the main selection criteria for some specific cases are described below.

*Scenario 1: Objects listed with an upper limit in the  $H$  or  $K$  bands.* The  $H$  band measurements are used uniquely in selection cut #1. There, if an object was to be selected at the brightness of the  $H$  upper limit value given, it would also remain selected for any fainter magnitude as the object would be shifted in the lower-right side of the IR colour-colour  $J - H$  versus  $H - K$  diagram used in cut #1. Therefore, using the  $H$  magnitude limit value as a classical measurement when we applied the seven main selection criteria described in Sect. 2.2.1 adds no biases to our selection. Concerning the  $K$  band, the situation is not the same as for fainter magnitudes than the upper limit value given, an object would shift to the left in the  $J - H$  versus  $H - K$  diagram and therefore could potentially come out the selection area. As we saw for ASAS-RCB-20, if an object misses only the  $K$  band measurement, the issue is most certainly due to a confusion between multiple sources and not to a non-detection. Therefore we used the  $K$  band value listed as such through all selection criteria.

*Scenario 2: Objects listed with an upper limit in the  $J$  band.* First, we did not keep objects that present an upper limit in the  $J$  band and are located near the Galactic centre and plane ( $|b| < 2$  deg and  $|l| < 60$  deg). We considered that the search of RCB stars in this highly crowded and extinguished area is better suited to the VISTA/VVV (Minniti et al. 2010) and *Spitzer*/GLIMPSE (Churchwell et al. 2009) datasets which have better spatial resolution. Then, outside that sky area, we decided to select objects that would pass all the seven main selection criteria listed in the previous section at the upper limit value given in the  $J$  band but also if they would be fainter by up to 1 mag. In practice, we decreased the  $J$  luminosity in 0.1 mag steps and tested all criteria each time. If an object was selected in all 11 steps (from 0 to 1 mag), it was validated for the next selection step. Furthermore, we requested that such objects present a unique possibility of association between the 2MASS and WISE catalogues, and that no blend was observed in WISE. On all six known RCB stars whose  $J$  band measurements present an upper limit, only three passed these criteria. The three rejected ones are: EROS2-LMC-RCB-6, EROS2-CG-RCB-5 and EROS2-CG-RCB-8. The candidate RCB star [RP2006] 1631, that is also listed with upper limit values in the  $J$  and  $H$  2MASS bands, did not pass our selection criteria either.

*Scenario 3: Objects listed with an upper limit only in the  $[22]$  band.* An object that would be fainter than the given  $[22]$  upper limit value would effectively have a bluer shell and would then move in the left side of the colour-colour diagram presented in Fig. 1. By shifting the reddest selection limit of cut #1 by 1 mag to the red:

$$[12]-[22] < 2.35 \quad \text{and} \quad [4.6]-[12] \geq 1.5 \times ([12]-[22]) - 1.45 \quad (6)$$

and applying the above criterion directly on the  $[22]$  upper limit values given, we have consequently widened the selection area and kept objects that could be up to one magnitude fainter than the  $[22]$  upper limit but still be potentially selected by the main selection criterion (see cut #2). We also added a more stringent shell brightness lower limit by requesting a strict brightness

<sup>1</sup> The typical completeness limits of the 2MASS catalogue are 15.8, 15.1 and 14.3 mag, respectively for the  $J$ ,  $H$  and  $K_s$  bands. It varies by one magnitude depending if observations were carried on towards the Galactic plane or at high Galactic latitude, because of the effects of confusion noise on the detection thresholds (Cutri et al. 2003).

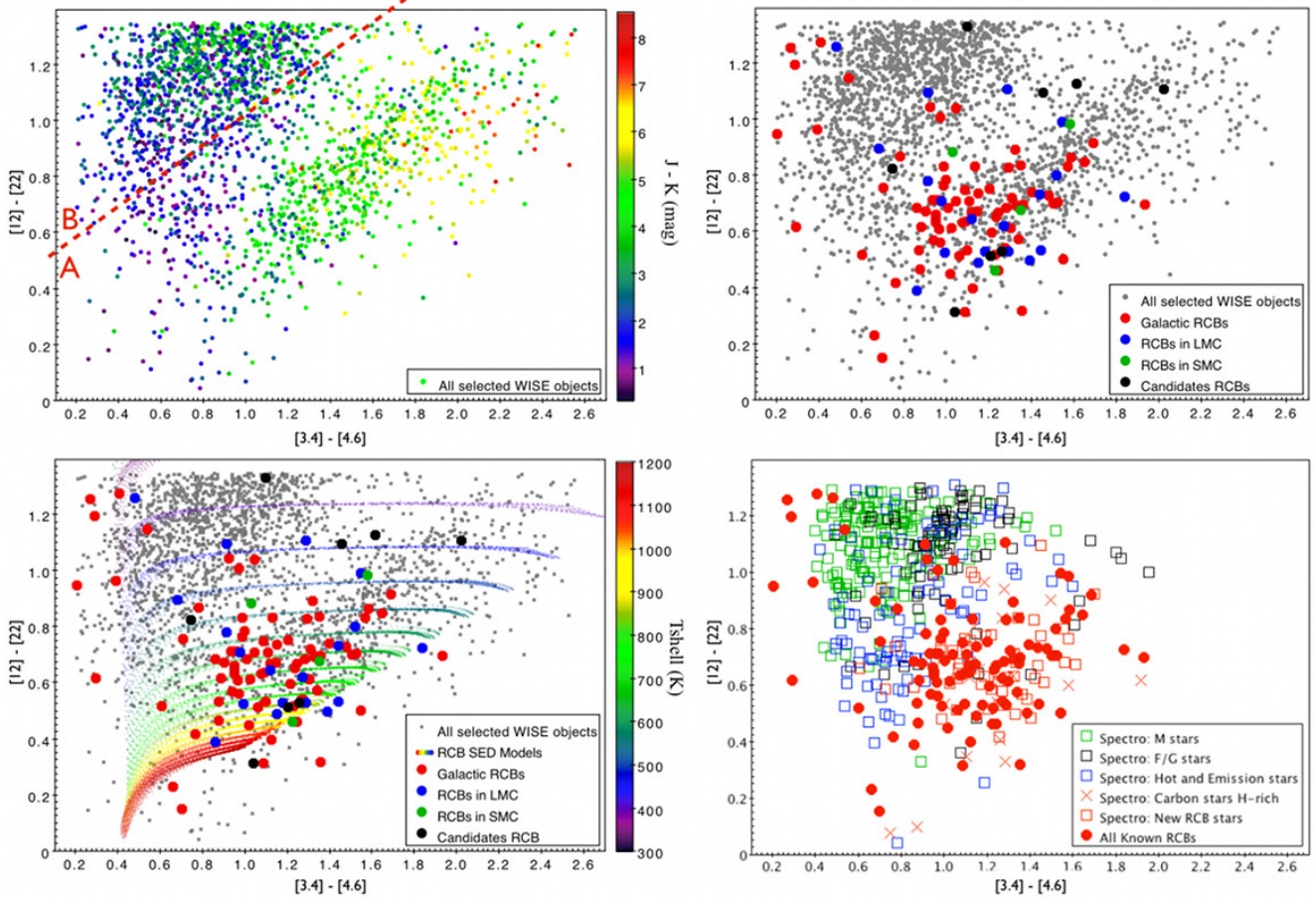


**Fig. 4.** Colour–colour  $[3.4] - [4.6]$  versus  $[12] - [22]$  diagrams. *Top-left:* distribution of all selected WISE targets of interest that have a valid measurement in all four WISE bands. The diagram is colour-coded with the  $J - K$  colour index. Two groups of objects are emerging; we are separating them pragmatically into two zones, A and B (see text for more details). *Top-right:* same sample of objects is represented in grey, while all known and candidate RCB stars are overlaid with large dots. Most RCB stars are located in zone A. *Bottom-left:* same diagram as the preceding except that the RCB SED models are added, colour coded with their shell temperatures. *Bottom-right:* here all known RCB stars are represented again by large red dots, while the large squares represent all the targets of interest that have already been followed-up spectroscopically. They are colour-coded respective to their spectral classifications.

threshold with  $[12] < 8$  mag in selection cut #4. Finally, no blend can be present in WISE and we added a stricter cut on the colour  $[4.6] - [12] < 3$  mag.

In conclusion, we added 469 targets of interest (397 Galactic, 72 Magellanic) to our final catalogue (about 20% of the total). They all present at least one upper limit value in the  $J$ ,  $H$ ,  $K$ ,  $[3.4]$  or  $[22]$  bands. Most of them will be listed in the low priority group #4 for spectroscopic follow-up (see Sect. 2.4).

### 2.3. Results

The summary of the selection criteria applied is stated in Table 1. Out of the sample of 101 Known RCB stars used as a reference, 14 were not selected by our analysis. It corresponds to a detection efficiency of  $\sim 85\%$ . Overall, the selection suits well typical RCB stars with effective temperatures between  $4000 < T_{\text{eff}} < 8000$  K and surrounded by a thick circumstellar dust shell with a temperature between  $400 < T_{\text{shell}} < 900$  K.

Using RCB SED models, we found that RCB stars that possess one of these three characteristics: (1) a cold circumstellar shell ( $T_{\text{shell}} < 400$  K), (2) a very thin shell as their SED would appear similar to classical F or G stars, or (3) a second colder

and thicker shell, like the one seen around MV Sgr (Tisserand 2012), have a low detection efficiency. Furthermore, we are less efficient at detecting RCB stars that possess a warm shell whose 2MASS epoch coincides with a large decline in brightness or are already affected by a high extinction due to any combination of interstellar and circumstellar dust. The first reason is that RCB stars may not be detected in 2MASS  $J$  or  $H$  passbands, or both, and secondly, even if they are detected, RCB stars with warm shells would be so red that they may exit the defined selection area defined (see cut #3 and Fig. 3).

Due to the low resolution of 2MASS and WISE surveys ( $>3$  arcsec) and the high interstellar extinction, our detection efficiency most certainly drops in the highly crowded central part of the Galactic bulge. We expect that it is strongly impacted in the sky area  $-2 < b < 2$  deg and  $-60 < l < 60$  deg where the interstellar dust extinction reaches  $A_K > 3$  mag. Higher resolution IR Surveys such as VISTA/VVV and Spitzer/GLIMPSE could be of great help to probe that crowded part of the sky.

Overall, out of 563 million objects catalogued by WISE, our final list of targets of interest, rich in RCB stars, contains 2356 objects, 2194 in the Galaxy and 162 in the Magellanic Clouds. Their distribution on the sky is presented in Fig. 16.

#### 2.4. Prioritisation for spectroscopic follow-up

The second stage of our search is to follow-up spectroscopically each of the candidates selected. For that task, we classified them into five different groups of increasing priority.

We considered as the lowest priority all targets that we found to have a genuine identification in the SIMBAD database. We classified them in Group #5. We carefully looked at the information reported for each object selected and marked the ones that either have already been reported with a spectral type, or have been classified as Mira/OH-IR stars from a radio survey or from optical photometric monitoring datasets with strong bibliographic support. We found also that our selection was contaminated by emission stars, RV Tauri stars and also some young stellar objects, T Tauri or pre-main sequence stars. Naturally, objects identified as carbon stars were not included in the low priority group as new observations with the same spectroscopic set-up as our on-going follow-up survey are necessary. We kept all objects from Group #5 in case of mis-classification. RCB stars are sometimes confused with Mira type stars as they both present light curves with large changes in luminosity (for example, MSX-LMC-1795 was classified as Mira in SIMBAD). Group #4 contains all objects that have been reported with an upper limit in at least one of the four WISE photometric bands or only in the 2MASS  $J$  band. We can expect that these objects are harder to follow-up as they could either be affected by a strong blending with neighbouring stars and/or have a strong extinction due to interstellar or circumstellar dust. At any given epoch, a fraction of RCB stars will be in a significant decline. Recently, the prototype R CrB returned to maximum light after a period of 9 years continuous decline, and V854 Cen was in a deep decline lasting at least 50 years before it was discovered (Kilkenny & Marang 1989; Lawson & Cottrell 1989).

The categorisation of the three highest priority groups is explained with the colour-colour  $[3.4]-[4.6]$  versus  $[12]-[22]$  diagrams presented in Fig. 4. In the top-left diagram, one can clearly recognise two distinct clumps of objects. We define two zones, A and B, to separate them. Interestingly, most of the known RCB stars are found in zone A (see top-right diagram). Using RCB SED models (bottom-left diagram), we understand that RCB stars located in zone B are the ones presenting a thin shell (therefore undergoing a low dust production phase) or having a thicker but colder shell than average ( $T_{\text{eff,shell}} < 500$  K), while, conversely, RCB stars with more typical warm thick shells are expected to be detected in zone A. Furthermore, looking at the distribution of objects classified as Mira or OH-IR stars in SIMBAD, or in our own on-going spectroscopic follow-up survey (see bottom-right diagram), we found that these stars occupy principally the top-left side of zone B. Therefore, we place all objects located in zone B in Group #3. As it contains the highest number of targets, but is also highly contaminated by Mira type stars and RV Tauri stars, further specific selection within that sample would therefore be useful to not misuse telescope time. However, the targets of Group #3 should not be disregarded as some less common RCB stars, that are useful to help to understand RCB's evolutionary path, can be discovered amongst them. Monitoring photometric surveys should be a very useful tool to detect and reject Mira type stars from this sample as their characteristic large periodic photometric oscillations are easily recognisable. RV Tauri stars are also expected to be present as some of them, the ones surrounded by dusty discs, show similar WISE colours (see Gezer et al. 2015).

For the two highest priority groups, we separated targets in zone A based on their  $J - K$  colour index as redder objects can be more difficult to follow-up due to high extinction, but

also because these redder targets are contaminated by extreme AGB stars (see cut #3 in Sect. 2.2.1 and Fig. 2). So, Group #1 includes all objects located in zone A and bluer than  $J - K < 3.5$  mag, and Group #2 includes all redder objects (see top-left diagram). Among the targets listed in priority Groups #2 and #4, are some intrinsically bright RCB stars, as they may have been observed in a high extinction phase during the 2MASS epoch and later returned to maximum light. They can also include uncommon highly-enshrouded RCB stars, such as MSX-SMC-014 and EROS2-SMC-RCB-4.

Group #1 contains only 375 targets (329 in our Galaxy and 46 in the Magellanic Clouds). We consider that it should hold the highest percentage of bona-fide RCB stars. Indeed, of the 87 known RCB stars that passed the selection criteria,  $\sim 70\%$  would be classified in Group #1, while only  $\sim 15\%$ ,  $\sim 12\%$ ,  $\sim 3\%$  would be classified in Group #2, #3 and #4 respectively. There are respectively 375, 463, 1005, 298 and 215 targets reported in Groups #1 to #5. An identification number is given to each target. This identifier was assigned depending on which location, Galactic or Magellanic, and which priority Group the target belongs to. As that corresponds to ten ensembles, each of them was given an interval of 1000 units between 1 and 10 000, starting at 1 for the Galactic sample and 5001 for the Magellanic one. For example, the Galactic (Magellanic) Group #1 targets are ranked between 1 (5001) and 1000 (6000), Group #2 between 1001 (6001) and 2000 (7000), etc.

#### 2.5. A new catalogue of candidate RCB stars

We compiled a new catalogue of targets of interest in our search for RCB stars using the all-sky 2MASS and WISE surveys. This new catalogue supersedes the one created by Tisserand (2012) using the WISE Preliminary data release. Further studies and spectroscopic follow-ups are now needed to classify each star. From the approximately 563 million objects catalogued by the WISE All-Sky survey, we have selected only 2356 targets (2194 in the Galaxy and 162 in the Magellanic Clouds) that present similar near- and mid-infrared colours and brightness to typical RCB stars. We used the 101 known RCB stars as a reference sample and determined a high detection efficiency of 85%. Furthermore, we found that the HdC star, HD 175893, also passed all our photometric selection criteria. It is in fact not surprising as HD 175893 is the only HdC star known to possess a circumstellar dust similar to RCB stars (Tisserand 2012). As we have a similar efficiency for selecting RCB stars in the Magellanic Cloud as in the Galactic sample, we conclude that our search should allow us to detect any RCB stars located within  $\sim 50$  kpc from the sun.

We present a short version of the RCB enriched catalogue in Table 2. The entire catalogue will be available through the Vizier catalogue service. Each target is listed with its identification number related to its priority group and its own WISE identification. Then in the following order, one will find their equatorial and Galactic coordinates, as well as all their four WISE and three 2MASS magnitudes with their associated 1-sigma errors. The last three columns of the catalogue give information listed by the SIMBAD (as of 2015-08-11) database using a 3 arcsec matching radius, for instance: name, object type and spectral classification. When no information was given, the number -99 is listed in replacement.

To simplify the coordination of the follow-up of each candidate, a dedicated web interface<sup>2</sup>, has been created to be able to monitor the status of each star and give access to all relevant

<sup>2</sup> <http://rcb.iap.fr/trackingrcb/>

**Table 2.** First 10 rows of the published catalogue.

ID	WISE ID	RA (deg)	Dec (deg)	$l$ (deg)	$b$ (deg)	WISE		WISE		WISE	
						[3.4] (mag)	$\sigma_{[3.4]}$ (mag)	[4.6] <sub>corr</sub> (mag)	$\sigma_{[4.6]}$ (mag)	[12] (mag)	$\sigma_{[12]}$ (mag)
1	J000842.12+630033.6	2.1755086	63.0093535	118.1051790	0.5388797	7.875	0.023	7.088	0.020	5.521	0.014
2	J001910.61+520203.5	4.7942272	52.0343285	117.8955721	-10.5215968	6.771	0.041	5.87827	0.026	4.603	0.015
3	J002921.18+644850.6	7.3382829	64.8140565	120.5838170	2.0431257	11.433	0.024	11.046	0.023	9.784	0.043
4	J003901.29+592805.0	9.7554102	59.4680639	121.3528413	-3.3655336	11.025	0.024	10.476	0.021	7.428	0.017
5	J004628.27+585420.8	11.6177924	58.9057907	122.2891557	-3.9596824	11.556	0.022	10.874	0.020	9.309	0.040
6	J004822.34+741757.4	12.0930919	74.2992817	122.7203357	11.4288814	6.679	0.040	5.17692	0.028	3.067	0.008
7	J004947.53+633810.0	12.4480736	63.6361242	122.7492110	0.7650405	9.247	0.023	8.343	0.021	6.871	0.018
8	J005128.08+645651.7	12.8670235	64.9477022	122.9351159	2.0760360	6.911	0.033	5.63923	0.029	3.876	0.015
9	J010500.10-054003.6	16.2504303	-5.6676941	132.0909095	-68.2979230	8.042	0.023	7.145	0.021	5.938	0.015
10	J013000.19+631044.5	22.5008221	63.1790352	127.2660314	0.6323574	10.320	0.024	9.821	0.020	8.673	0.030
Columns continued											
WISE		2MASS		2MASS		2MASS		SIMBAD			
[22] (mag)	$\sigma_{[22]}$ (mag)	$J$ (mag)	$\sigma_J$ (mag)	$H$ (mag)	$\sigma_H$ (mag)	$K$ (mag)	$\sigma_K$ (mag)	Name	Object type	Spectral class	
4.622	0.024	10.285	0.018	9.603	0.017	9.059	0.020	-99	-99	-99	
4.163	0.023	9.501	0.022	8.192	0.017	7.187	0.018	V* V858 Cas	sr*	-99	
9.178	0.517	12.923	0.024	12.465	0.031	11.947	0.026	-99	-99	-99	
7.318	0.097	13.939	0.024	12.983	0.021	12.104	0.021	-99	-99	-99	
8.722	0.281	12.931	0.023	12.704	0.033	12.389	0.023	-99	-99	-99	
2.200	0.014	10.286	0.023	8.990	0.027	7.642	0.024	2MASS J00482232+7417574	IR	-99	
6.126	0.049	11.135	0.024	10.733	0.030	10.208	0.020	-99	-99	-99	
3.367	0.022	10.936	0.027	10.066	0.030	9.177	0.019	IRAS 00483+6440	*	-99	
5.654	0.038	10.643	0.024	9.386	0.025	8.378	0.025	[BEM91] 7	C*	C	
8.000	0.261	11.329	0.022	10.774	0.028	10.248	0.025	-99	-99	-99	

**Notes.** The full table is available at the CDS.

information: available light curves, spectra and/or observing charts. The authors invite everyone to report any information that would help them to identify new RCB stars. As of today, we have information that 313 of the candidates are Mira-type stars from their light curves or spectra. These targets do not need additional follow-up and their status is indicated on the website.

### 3. Spectroscopic data, light curves, and models

#### 3.1. Spectroscopic data

The spectroscopic follow-up of the ToI, listed above, was conducted with four telescopes. Table 4 lists the characteristics of the spectra obtained. Predominantly, we used the Wide Field Spectrograph (WiFeS) instrument (Dopita et al. 2007) attached to the 2.3 m telescope of the Australian National University at Siding Spring Observatory (SSO). WiFeS is an integral-field spectrograph permanently mounted at the Nasmyth A focus. It provides a  $25'' \times 38''$  field of view with  $0.5''$  sampling along each of the twenty-five  $38'' \times 1''$  slitlets. The visible wavelength interval is divided by a dichroic at around 600 nm, feeding two essentially similar spectrographs. The spectra have a two-pixel resolution of  $2 \text{ \AA}$  and wide wavelength coverage, from 340 to 960 nm. We observed 415 targets with WiFeS during eight observational runs: 20–25 July 2011, 4–7 June 2012, 23–25 July 2012, 1–3 August 2012, 23–30 July 2013, 15–18 and 24 August 2013. We also observed 61 targets with the Goodman spectrograph mounted on the 4.1 m Southern Astrophysical Research (SOAR) telescope located at Cerro Pachón, Chile on 6–8 July 2013. The  $6001 \text{ mm}^{-1}$  grating was used to achieve a  $1.3 \text{ \AA}$  two-pixel resolution with a 435–702 nm wavelength coverage using the GG-385 blocking filter. All of the data were reduced using the spectral reduction package FIGARO. The telluric lines were removed using the IRAF task, TELLURIC, and standard stars observed during our runs. All spectra were flux calibrated using standard stars observed during the night. We also observed seven targets

in automatic mode with the FRODOSpec instrument mounted on the 2 m Liverpool telescope at the Observatorio del Roque de los Muchachos. Using the low-resolution gratings, FRODOSpec can obtain the spectra of northern targets between 390 and 940 nm with a two-pixel resolution of  $4 \text{ \AA}$ . Six Magellanic targets were observed with the AAOmega double-beam multi-fibre spectrograph (Sharp et al. 2006) mounted on the 3.9 m Anglo Australian Telescope (AAT) at SSO as part of an observational campaign by Kamath et al. (2014, 2015).

#### 3.2. Light curves

The photometric data accumulated by monitoring surveys are also of great importance for our search as RCB star light curves show very characteristic photometric brightness changes. In particular, RCB stars are well known to undergo unpredictable fast and deep declines in brightness due to newly formed dust clouds that obscure the photosphere (up to nine magnitudes in  $V$  band) in only two or three weeks. The photosphere usually reappears slowly after a few months when the dust grains disperse due to radiation pressure (e.g. Clayton et al. 2013). However, in some cases, continual dust formation can keep the star in a deep decline for many years. If such fast and deep declines are observed for an RCB star candidate that also presents a carbon-rich spectrum, we use this information to strengthen our decision on its RCB nature. Furthermore, light curves allow us to remove some targets from the candidate list for spectroscopic follow-up, as they show periodic photometric variations typical of Mira and RV Tauri stars. This knowledge allows us to make more efficient use of telescope time.

Here is the list of monitoring surveys whose data were used for the present analysis: OGLE (Udalski 2003), CRTS (Drake et al. 2009), ASAS (Pojmanski 1997), and the Bochum survey (Hackstein et al. 2015). The OGLE light curves of some new RCB stars presented in this article will be published in a dedicated article by Przemek et al. (in prep.).

**Table 3.** Priority classification of the WISE Targets of Interest followed-up spectroscopically.

Priority Id for follow-up	ToI Ids Galactic, Magellanic	Number of ToI	
		Galactic (with conclusive spectra) (with clear non-RCB variability) New RCB stars / candidates	Magellanic
1	1–1000,	329	46
	5001–6000	(135) (6) 31/13	(10) (19) 4/0
2	1001–2000,	456	7
	6001–7000	(36) (12) 6/0	(1) (5) 1/0
3	2001–3000,	987	18
	7001–8000	(248) (143) 1/0	(8) (1) 0/0
4	3001–4000,	247	51
	8001–9000	(0) (7) 0/0	(0) (12) 0/0
5	4001–5000,	175	40
	9001–10 000	(41) (18) 0/1	(9) (11) 0/0
	No Id	– (–) (–) 2/1	– (–) (–) 0/0
	Total	2194 (460) (186) 40/15	162 (28) (48) 5/0

**Notes.** See Sect. 2.4 for a summary of the prioritisation process.

### 3.3. Atmospheric models

Finally, we used a grid of hydrogen-deficient and carbon-rich MARCS (Model Atmospheres in Radiative and Convective Scheme) atmospheric models for various  $T_{\text{eff}}$  (from 4000 to 7500 K), surface gravities ( $\log g = 0.5$  or  $1.0$ ), and nitrogen abundances ( $[N]$  from 7.0 to 9.4) (Gustafsson et al. 1975, 2008; Bell et al. 1976; Plez 2008). We then created synthetic spectra using the Turbospectrum program (Alvarez & Plez 1998; Plez 2012) and the Vienna Atomic Line Database (VALD) (Ryabchikova et al. 2015) to get information on atomic and molecular transition parameters.

## 4. Spectroscopic analysis

First, we searched for our 2356 ToI in the databases of the monitoring surveys listed above. We found that light curves were available for 510 of them (394 Galactic and 116 Magellanic ToIs), and that 234 show typical photometric oscillations of large periodic variable stars such as Miras (226) and RV Tauri stars (8). We therefore did not observe these ToI spectroscopically to save telescope time, except for 35 ToI where the spectroscopic follow-up was done before the light curves became available.

We have obtained spectra of 488 targets so far. A detailed summary of the number of spectra obtained for each priority group, as well as the number of objects presenting light curve with large periodic variability unseen in any known RCB stars,

**Table 4.** Characteristics of the spectra obtained.

Telescope	Spectrograph	Wavelength range (nm)	Two-pixel resolution (Å)
SSO/2.3 m	WiFes	340–960	2
SOAR/4.1 m	Goodman	435–702	1.3
Liverpool/2 m	FRODOSpec	390–940	4
AAT/3.9 m	AAOmega	370–880	3

is given in Table 3. We immediately recognised and discarded 263 stars that present non-RCB spectra. Among those, 189 presented spectra of oxygen-rich M stars (Miras), with typical wide absorption features due to the TiO and VO molecules. The large majority of these stars belong to priority group #3. In the Magellanic Clouds, the number of these targets is low because of the special selection criteria based on the  $K$  versus  $J-K$  H-R diagram, implemented early on to remove most Magellanic Mira-type objects (see cut #5 in Sect. 2.2.1). Another 74 were found to have spectra of hot, hydrogen-rich stars. All of these rejected stars are listed in our dedicated search website<sup>3</sup>.

To classify new RCB stars among the remaining spectra collected, we sorted the spectra into four groups, as RCB stars present a variety of optical spectra. Classical RCB stars are known to possess a wide range of  $T_{\text{eff}}$ , from about 4000 to 8500 K, as they evolve through the H-R diagram. Indeed, below  $\sim 6800$  K, one can clearly observe absorption bands due to the  $C_2$  and CN molecules (see Figs. 5–7). These bands strengthen with lower  $T_{\text{eff}}$ . Above the temperature threshold, none of these molecules exist and the spectra consist of atomic absorption lines (Fe I, C I, N I and O I, Ca II, in particular – see Figs. 10 and 11 for some examples). So, we classified our observed ToI into two distinct groups, cold and warm RCB stars (Sects. 4.1 and 4.2), based on the presence or absence of the molecular bands in their spectra. We also added two further ToI groups to search for RCB stars presenting spectra with emission lines. The first group has characteristic emission lines seen when an RCB star undergoes a decline (Sect. 4.3). The second group represents rare Hot RCB stars ( $T_{\text{eff}} > 15\,000$  K) that present spectra with many strong emission lines (Sect. 4.4).

We have defined and applied specific selection criteria for each of these four groups. These criteria are described in detail in the subsections below. A fifth and last group should also be mentioned, which is only seen when an RCB star is observed during a very deep minimum of a decline. In that particular scenario, only the cold and featureless spectrum of the circumstellar dust shell will be observed. We will discuss that particular case within the decline group (Sect. 4.3).

Finally, it is worth underscoring here that the vast majority of classical giant carbon stars were excluded during the IR selection process. Only extreme carbon-rich AGB stars are expected to be found within our ToI classified in priority groups #2 and #4. These groups were formed to contain ToI that are highly obscured due to thick circumstellar dust ( $J - K > 3.5$  mag) and therefore potentially more difficult to observe and identify.

All newly discovered RCB stars and all new candidates are listed in Table B.1.

### 4.1. First group: Cold RCB stars

We focus here on a group of 72 ToI that show strong band-head features due to  $C_2$  and CN, observable in the blue and red of the optical. Cold RCB stars have a  $T_{\text{eff}}$  ranging between  $\sim 4000$

<sup>3</sup> <http://rcb.iap.fr/trackingrcb/>



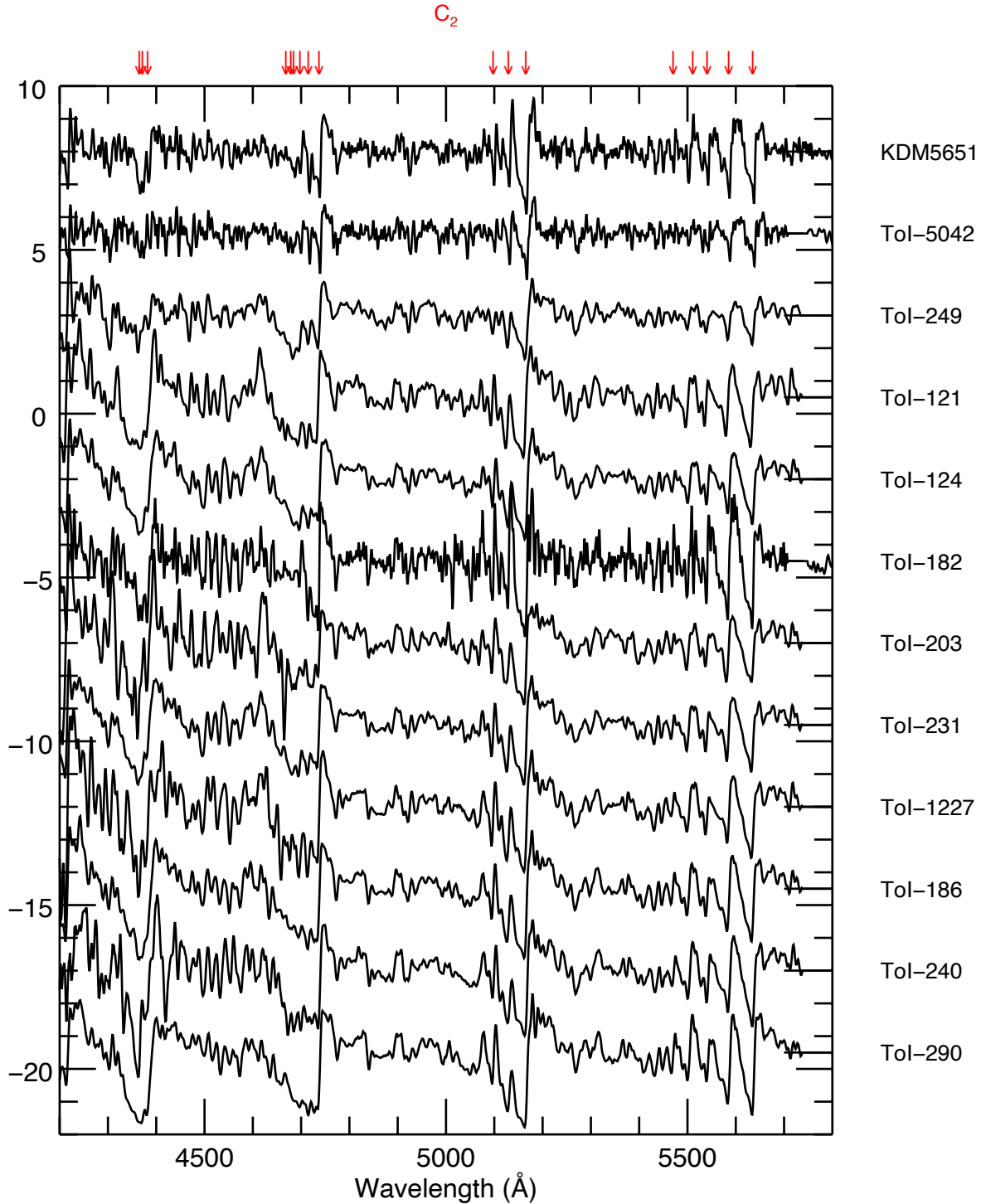


**Fig. 6.** Spectra, blue region from 4200 to 5800 Å, of KDM 5651 and a selection of 11 newly discovered Galactic Cold RCB stars that present the best signal-to-noise ratio. The underlying blackbody curves were removed. The large C<sub>2</sub> band-heads features (2,0), (1,0), (0,0) and (0,1) are clearly visible. We plotted them in order of the Ca II IR triplet strength, from stronger to weaker lines (top to bottom), that is, in decreasing order of  $T_{\text{eff}}$ . The spectra were smoothed (5 points were used) for a better presentation and comparison. The names of the corresponding stars are given on the right side.

very weak CN features in their respective spectra. From further studies of these spectra as well as the near IR photometry, they suggested that five of them are strong Magellanic RCB candidates and the sixth, KDM 6546, presenting slightly stronger CN bands, should probably be a Galactic halo CH star located in front of the Large Magellanic Cloud. At the time, due to the lack of light curves and the narrow wavelength coverage of the

spectra, the nature of these six stars remained unconfirmed. An update on their classification status is given in Table 5.

All five stars listed as strong Magellanic RCB star candidates by Morgan et al. (2003) are now confirmed RCB stars. It underscores that the spectroscopic analysis criteria described in Morgan et al. (2003, Sect. 4 and references therein) can be considered a very reliable method for identifying new RCB

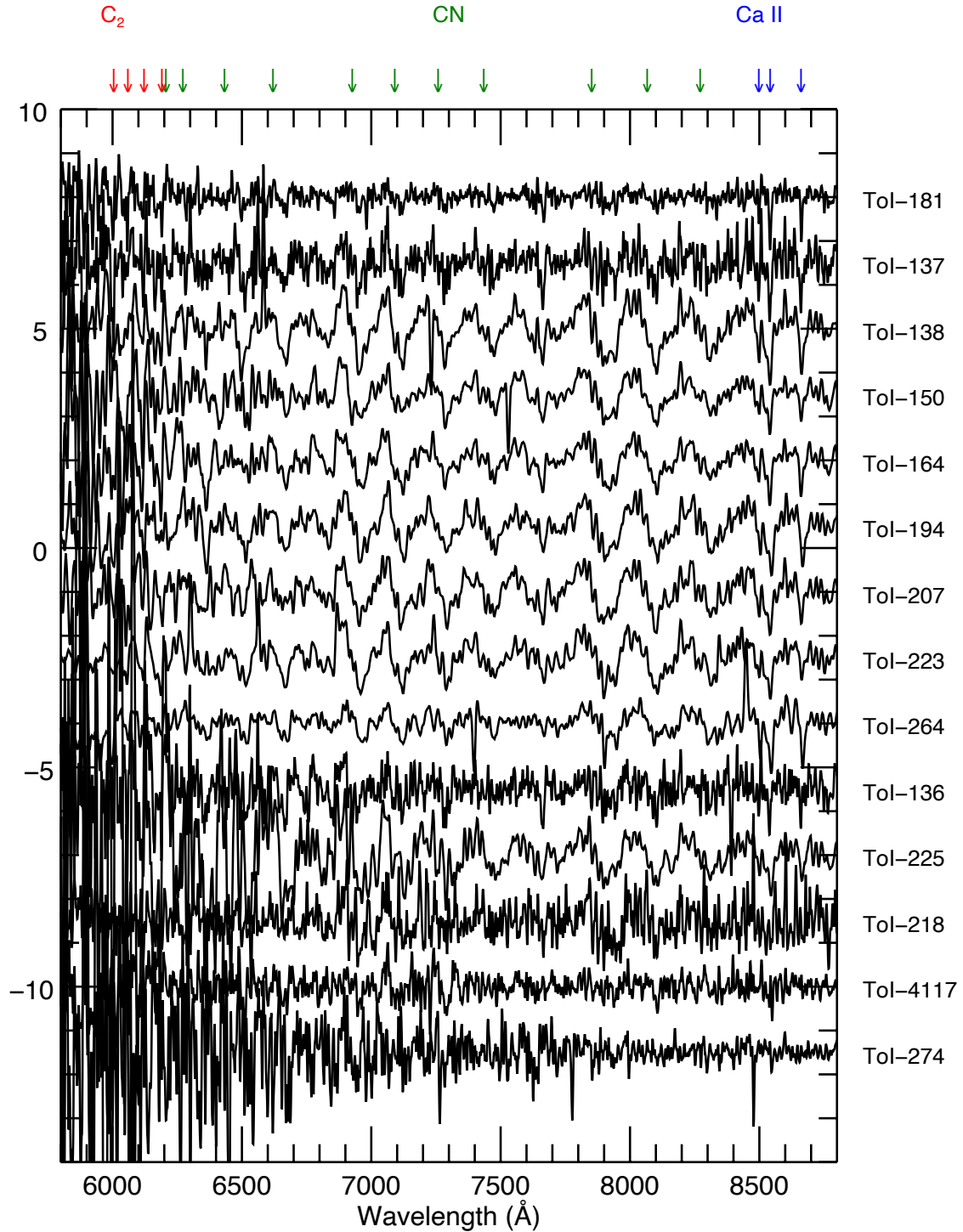


**Fig. 7.** Spectra, red region from 5800 to 8800 Å, of the 14 new strong Cold RCB candidates found in this study. The underlying blackbodies curve were removed. The spectra were smoothed (5 points were used) for a better presentation and comparison. The names of the corresponding stars are given on the right side. They are strongly suspected to have been observed during dust obscuration events. We plotted them in order of their Ca II IR triplet strength, from stronger to weaker lines (top to bottom).

stars. Here are the main criteria: firstly, very weak CN bands detected allowing four strong  $C_2$  bands to be clearly distinguished between 6000–6200 Å, secondly, no hydrogen Balmer lines detected, and thirdly, no  $^{13}C$  features observed.

Furthermore, the spectral analysis was supported by the study of each CN-weak star’s near-IR luminosity and colour in comparison with other more classical carbon stars and already known RCB stars. [Morgan et al. \(2003\)](#) showed that the known

RCB stars stand out compared to the classical carbon stars locus, but also more interestingly that the five candidates follow the same near-IR characteristics as RCB stars.

All but one, KDM 5651, have passed our photometric selection criteria. KDM 5651 would have been selected if, as mentioned in Sect. 2.2.1, cut #2, its [22] WISE ALL-Sky measurement had not been strongly biased. Interestingly also, the Galactic CH star, KDM 6546, was rejected as it did not

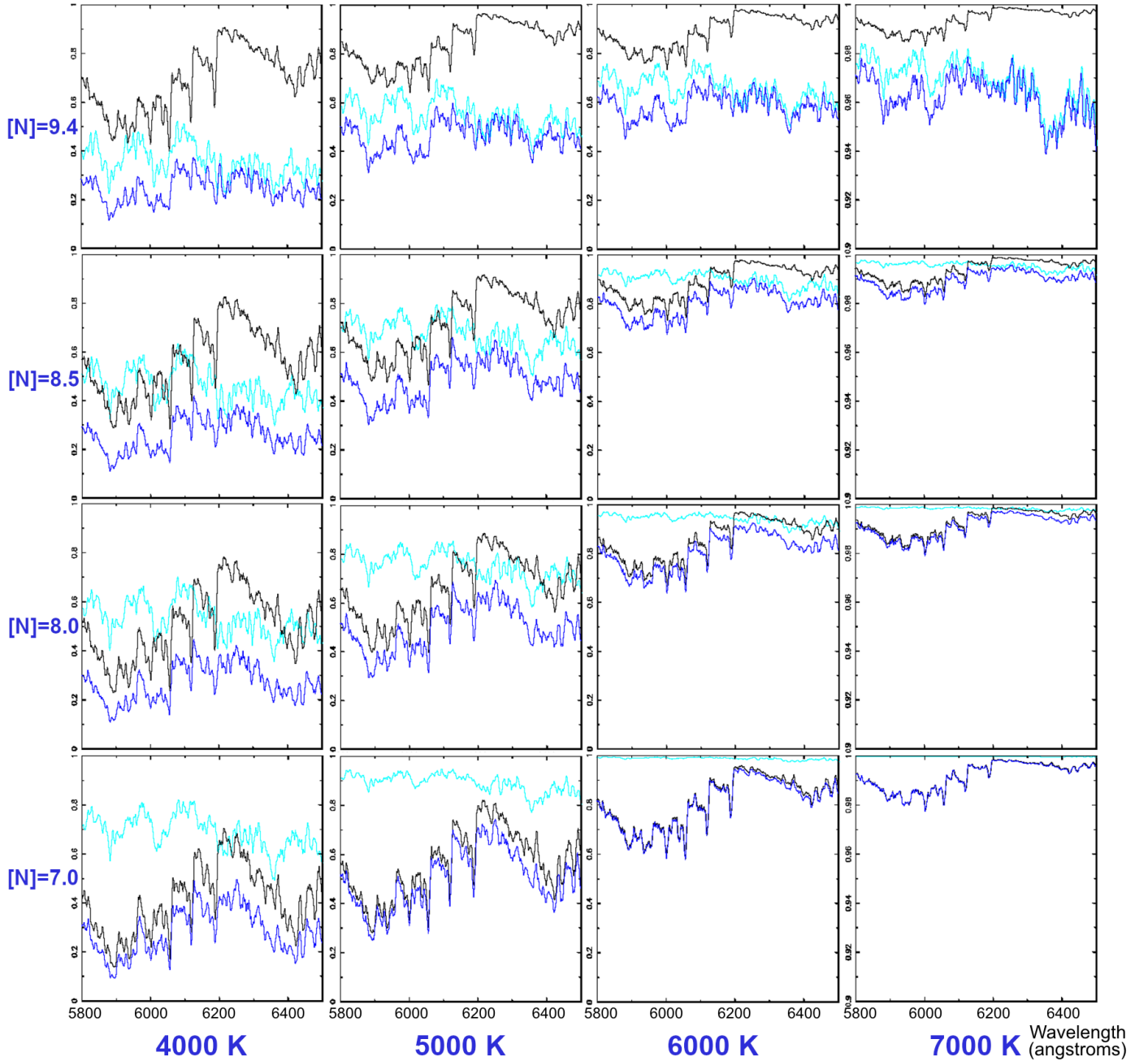


**Fig. 8.** Hydrogen-deficient synthetic spectra between 5800 and 6400 Å for four different nitrogen abundances ( $7.0 \leq [N] \leq 9.4$  dex) and four different  $T_{\text{eff}}$ s (4000 to 7000 K). The spectra are normalised to unity. The intensity scales extend between 0 and 1 for all spectra except the ones with a  $T_{\text{eff}}$  of 7000 K whose intensity scales are between 0.9 and 1. Cyan represents the CN band-head features, black represents the C<sub>2</sub> bands, and blue is the sum of both. The abundances used for the models are those of a classical RCB star, i.e. [H] = 7.5, [He] = 11.5, [C] = 9.0 and [O] = 8.8, and the C/N ratio increased ( $\sim 0.4$ ,  $\sim 3.0$ , 10, and 100) by decreasing the nitrogen abundances.

pass the first two selection criteria using near- and mid-IR colours.

#### 4.1.2. Our selection of Cold RCB stars

Dust reddening effects made the spectroscopic analysis of this cooler group of stars more difficult. In many cases, most of the signal detected was concentrated on the red side of the spectra, and some important features located in the blue ( $\lambda < 5500$  Å) was missing. In particular, these include the CH molecular band at  $\sim 4300$  Å (only 11 out of the 73 cold ToI have some signal that

far into the blue), but also, the (1,0)  $^{13}\text{C}^{12}\text{C}$  absorption line at 4744 Å and the nearby (1,0)  $^{12}\text{C}^{12}\text{C}$  at 4737 Å. Fortunately, the  $^{13}\text{C}$  abundance can also be estimated from the red side of the spectrum with the (1,3) and (0,2)  $^{13}\text{C}^{12}\text{C}$  bands, respectively at 6100 and 6168 Å, which are near a series of  $^{12}\text{C}^{12}\text{C}$  bands, and also the  $^{13}\text{CN}$  band-head at  $\sim 6260$  Å with the nearby (4,0)  $^{12}\text{CN}$  band-head at 6210 Å if nitrogen abundance is high enough for the CN bands to be detectable. Most RCB star atmospheres are known to have a high C/N abundance ratio and a low  $^{13}\text{C}/^{12}\text{C}$  isotopic ratio, but this is not always the case (Rao & Lambert 2008; Hema et al. 2012).

**Table 5.** Status on RCB stars candidates listed by [Morgan et al. \(2003\)](#).

Names	Location	Classification	Comments
RAW 21, EROS2-SMC-RCB-1	SMC	RCB confirmed	A decline was observed in its EROS-2 light curve and no CH band was observed at 4300 Å ( <a href="#">Tisserand et al. 2004</a> ).
KDM 2373, EROS2-LMC-RCB-2	LMC	RCB confirmed	A slow decline phase was observed by the MACHO survey as already reported by <a href="#">Morgan et al. (2003)</a> . This decline and the following recovery were observed in its EROS2 light curve and no CH band was observed ( <a href="#">Tisserand et al. 2009</a> ).
KDM 5651	LMC	RCB confirmed	A series of small declines were observed by the three microlensing surveys, MACHO, EROS-2 and OGLE. A decline of ~0.3 mag at JD~2450200 was detected by MACHO, then subsequently two similar declines of ~0.3 mag were also monitored by EROS-2 at JD~2451800 and ~2452100. The recovery stage of that last decline was observed by OGLE-III (see <a href="#">Soszyński et al. 2009</a> , OGLE-LMC-RCB-20). About ~11.8 years later, a stronger decline of ~1.7 mag was observed by the OGLE-IV RCOM survey <sup>(a)</sup> . We obtained a spectrum during our observational campaign and no CH band was observed, confirming a previous analysis made by <a href="#">Hartwick &amp; Cowley (1988)</a> of their candidate HC 119 spectrum. We observed absorption features due to C <sub>2</sub> and CN molecules typical of Cold RCB stars.
KDM 2492	LMC	RCB confirmed	This is the already identified Magellanic RCB star, HV 5637 ( <a href="#">Alcock et al. 2001</a> ). No decline was observed for more than 20 years between the MACHO, EROS-2 and OGLE-III microlensing surveys, but a ~2.4 mag decline was monitored by the OGLE-IV RCOM monitoring system.
KDM 7101, EROS2-LMC-RCB-5	LMC	RCB confirmed	Two large and rapid declines were observed by the EROS-2 survey ( <a href="#">Tisserand et al. 2009</a> ). No CH band was observed.
KDM 6546	Galactic	Confirmed CH star	We obtained a spectrum during our observational campaign and detected a strong CH band-head at ~4300 Å (see Fig. 9). It was already reported as a CH star by <a href="#">Hartwick &amp; Cowley (1988)</a> , HC 193, but as discussed by <a href="#">Morgan et al. (2003)</a> , there was a possible issue due to a positional mismatch of more than 30''.

**Notes.** <sup>(a)</sup>See OGLE-IV RCOM (OGLE Monitoring system of R Coronae Borealis type variable stars) website: <http://ogle.astrouw.edu.pl/ogle4/rcom/kdm-5651a.html>

It has always been possible to detect the presence or absence of Balmer lines to test for hydrogen deficiency. RCB stars generally show weak or absent Balmer lines, but at least one RCB star, V854 Cen, shows significant hydrogen lines ([Lawson & Cottrell 1989](#); [Kilkenny & Marang 1989](#)). It is also now possible to detect the Ca II IR triplet located in the red ( $\lambda \sim 8498, 8543$  and  $8662$  Å). Indeed, the intensity of these lines is, as shown by [Richer \(1971\)](#), a good indicator of carbon star temperature: the cooler the temperature, the weaker the lines. We have therefore empirically classified each of the 73 candidate RCB stars based on the Ca II IR triplet strength: none, weak, small, medium, and strong.

The CN bands observed in RCB stars are weaker than the ones observed in classical carbon stars. As discussed in the previous section, this allows the possibility of detecting four C<sub>2</sub> band-heads between 6000 and 6200 Å that are normally swamped by strong CN bands nearby. We studied synthetic spectra for a range of  $T_{\text{eff}}$  and C/N abundance ratios, and found that these C<sub>2</sub> bands indeed become detectable when the C/N ratio is higher than 3 and the  $T_{\text{eff}}$  ranges between 5000 and 6000 K (see Fig. 8). The second C<sub>2</sub> band-head, around 6000–6060 Å, fades first with a higher nitrogen abundance due to a strong CN band-head appearing nearby. At higher temperatures, ~6000 K, the four C<sub>2</sub> band-heads can be seen even for lower C/N ratios as the CN bands

vanish. On the other hand, at a low temperature like ~4000 K, the C/N ratio needs to be higher than 100 to begin to observe these band-heads. For a large majority of Cold RCB stars, the observation of these C<sub>2</sub> features, rarely seen in classical carbon stars, are therefore common and can be used as a simple identification criterion. This criterion is not infallible, so for a very few RCB stars, like V4017 Sgr, there are no C<sub>2</sub> band-heads that are easily detectable in this wavelength range. We also note that after looking closely at the spectra of known RCB stars, we found that selecting stars based only on the extreme weakness of the CN bands, as did [Morgan et al. \(2003\)](#), was too strict a criterion to detect all of the RCB stars.

Using already known RCB stars and synthetic spectra matching their  $T_{\text{eff}}$ , we established a series of criteria to reveal new RCB stars. We describe these criteria below.

Among the 73 cold candidates, we recognised that 13 of them show H <sub>$\alpha$</sub>  emission indicating that they are not hydrogen-deficient. They are most certainly carbon-rich AGB stars which show a cooler  $T_{\text{eff}}$  than RCB stars ( $T_{\text{eff}} < 3500$  K). This is confirmed by the strength of the Ca II IR triplet which is non-existent. These stars also present a very high IR excess and are located in the extreme top-right of the  $J-H$  versus  $H-K$  colour-colour diagram presented in [Tisserand \(2012, Fig. 6\)](#), where AGB carbon-rich stars are expected to be found. We rejected

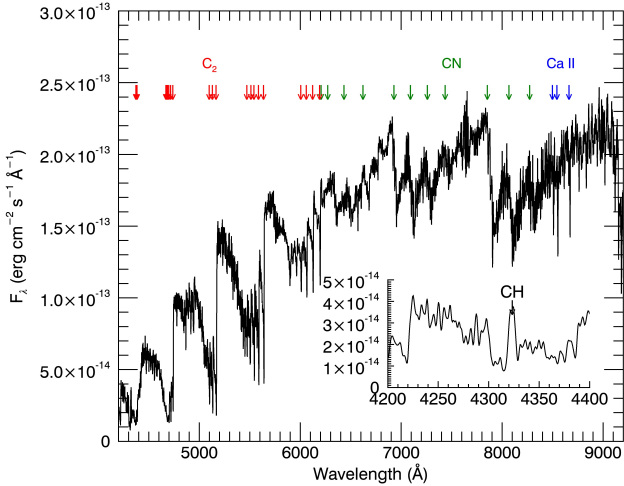


**Fig. 9.** Spectrum of KDM 6546 from 3400 to 9600 Å as observed on 2012-10-02 with the 2.3 m/WiFeS spectrograph and  $R \sim 3000$  resolution. The CH band-head between 4280 and 4310 Å is clearly visible (see insert spectrum). We confirm the first speculation that KDM 6546 is indeed a Galactic halo CH star located in front of the Large Magellanic Cloud (Morgan et al. 2003). The four consecutive  $C_2$  band-heads between 6000–6200 Å are visible also in the KDM 6546 spectrum as its C/N ratio is higher than classical carbon stars.

these stars. Another seven stars present strongly reddened spectra, but no  $H_\alpha$  emission. These are also carbon stars due the presence of CN bands at wavelengths longer than 7900 Å. They also show no Ca II IR triplet. So, these objects are most certainly carbon-rich AGB stars. We do not consider them further in our analysis.

Of the 60 remaining targets, 53 of them do not show any  $H_\alpha$  emission or CH absorption. First, we focused on the 40 warmer ones, which are the ones showing Ca II IR triplets classified as small, medium, or strong. They are interesting ToI as RCB stars are known to be warmer than classical carbon stars. Among them, we recognise that 27 presented some  $C_2$  features between 6000–6200 Å and no substantial  $^{13}\text{C}$  signal. We consider all these 27 stars as new bona fide RCB stars. Moreover, for eight of them, we even had enough signal in the blue spectrum to confirm the absence of the CH band which strengthens their identification. They are our “golden” Cold RCB sample as they match all of the following criteria: pass the near- and mid-IR photometric RCB selection, have a warm  $T_{\text{eff}}$  based on Ca II strength, no  $H_\alpha$  emission or CH band detected,  $C_2$  features between 6000–6200 Å observed and no substantial amount of  $^{13}\text{C}$  found. Finally, we found light curves showing characteristic RCB star declines for nine out of these 27 new bona fide RCB stars.

Second, we looked at the other group of 13 cooler candidates, presenting only weak or absent Ca II IR triplets. Their classification revealed to be more difficult as many of these stars show very noisy spectra at the interesting 6000–6200 Å wavelength range. However, first, we identified three ToI, numbers 90, 290, and 5039, presenting spectra with the same characteristics as listed above for the warmer RCB stars. Moreover, their CN bands were found to be very weak and typical RCB light curves were obtained for ToI 290 and 5039. We include all three of them in our list of new bona fide RCB stars. ToI 90 and 290 can also be included in our Cold “golden” sample as no absorption from CH molecules was detected.

Then out of the remaining ten cooler candidates, we kept seven of them: numbers 136, 138, 150, 164, 181, 207, and 225.

They should remain as RCB candidates, as further analysis and observations will be needed before final confirmations can be made. These stars present very similar red carbon-rich spectra with the following characteristics: no detectable signal in the blue, low fluxes in the  $C_2$  region of interest (6000–6200 Å) and visible CN bands at wavelengths longer than 6900 Å. It was also impossible to determine the abundance of  $^{13}\text{C}$ . Nevertheless, we found that the two strongest  $C_2$  band-heads, (0,2) and (1,3), were visible in all cases and that CN bands around  $\sim 6210$  Å seem very weak or non-existent. They have weak Ca II IR triplet absorption and no  $H_\alpha$  was detectable (except for ToI 136, which shows  $H_\alpha$  and [O I] at 6300 Å in emission). Interestingly also, we note that all these ToI are part of the high priority group #1, a group where no classical AGB carbon-rich stars are expected to be found.

Now we discuss the particular case of ToI 218, also belonging to the priority #1 selection group. It also presents a very red spectrum and as for the previous seven stars, we could not determine its abundance of  $^{13}\text{C}$  or the presence or absence of CH, but again no  $H_\alpha$  in absorption or emission was found indicating hydrogen-deficiency. The main difference is that ToI 218 shows no Ca II IR triplet at all and no sign of  $C_2$  features but only wide CN features at wavelengths longer than 6900 Å. Based on these characteristics, we would not have kept this star as a strong RCB candidate; however, there are light curves from the EROS-2 and OGLE surveys showing characteristic RCB-like declines. As discussed above, detecting the  $C_2$  features around the 6000–6200 Å region is a common observation for Cold RCB stars but it is not mandatory as already seen with the known RCB, V4017 Sgr. These  $C_2$  features are harder to detect at temperatures as low as 4000 K (see Fig. 8) as it would need a higher C/N ratio. Then, ToI 218 could indeed be an RCB star with a low  $T_{\text{eff}}$ , as indicated by the absence of the Ca II IR triplet. Another possible explanation for the absence of these Ca II absorption lines is that we could have observed ToI 218 in a decline phase and therefore emission in the Ca II lines fill in the absorption lines. More details on emission lines observed in Cold RCB spectra are discussed in Sect. 4.3 below. We need to obtain another spectrum, perhaps at a brighter phase, to definitely confirm the status of ToI 218. We list it as a strong candidate.

The spectra of all new RCB stars are presented in Figs. 5 and 6 in decreasing order of the Ca II IR triplet strength (i.e. in decreasing order of  $T_{\text{eff}}$ ). One can see that the  $C_2$  features in the interesting region between 6000 and 6200 Å are visible in all cases, but also that the next five  $C_2$  band-heads located between 6500 and 6900 Å are getting stronger with the decreasing effective temperature. The strength of the CN band around  $\sim 6210$  Å is different for each new RCB star, confirming that selecting RCB stars based on the extreme weakness of the CN bands cannot be a strong selection criterion. For example, the CN band around  $\sim 6210$  Å is weak for ToI 290 and 5039, but much stronger in the case of ToI 1220 and 1241.

Finally, we note that ToI 5042, a member of our “golden” Cold sample, shows absorption bands due to  $C_2$  and CN, as well as many absorption lines that are typical of Warm RCB stars. We discuss these lines below. ToI 5042 is the warmest of our 30 Cold new RCB stars (see Figs. 5 and 6).

#### 4.2. Second group: Warm RCB stars

Molecules do not exist in the atmospheres of RCB stars whose temperatures exceed  $\sim 6800$  K. Therefore, only atomic absorption lines of abundant elements, predominantly C I, N I, O I, but also Fe I, are seen in their spectra. In Fig. 10, we present

**Table 6.** Spectroscopic analysis of new Cold RCB stars.

WISE ToI	WISE [12] (mag)	2MASS K (mag)	Ca II IR triplet strength	<sup>13</sup> C ? ~4744, ~6168 Å	Strength C <sub>2</sub> features 600–620 nm	Hydrogen ? H <sub>α</sub> , CH	Emission lines ? (Å)	Comments
New Cold RCB stars								
76	3.55	8.32	Medium	n/a, No	Strong	No, n/a		
90	5.04	8.82	None	n/a, No	Strong	No, No		
105	4.41	9.46	Medium	n/a, No	Small	No, n/a		
121	4.10	8.54	Medium	No, No	Strong	No, No		
124	4.96	9.20	Medium	No, No	Strong	No, No		
130	2.22	8.04	Small	n/a, No	Small	No, n/a		
148	5.07	9.26	Small	n/a, No	Strong	No, n/a		
161	4.68	8.84	Small	n/a, No	Strong	No, n/a		
177	2.87	7.86	Medium	No, No	Strong	No, n/a		
182	3.22	7.44	Medium	No, No	Strong	No, No		
184	3.64	8.50	Small	n/a, No	Small	No, n/a		
186	4.46	8.65	Small	No, No	Strong	No, No		
203	4.76	8.37	Medium	No, No	Strong	No, No		
204	3.10	8.13	Small	n/a, No	Strong	No, n/a		
220	7.04	9.72	Medium	No, No	Strong	No, n/a		
231	5.34	9.72	Medium	No, No	Strong	No, No		
240	3.54	7.48	Small	No, No	Strong	No, n/a		
249	3.66	7.56	Strong	No, No	Strong	No, No		
250	3.68	8.67	Small	No, No	Strong	No, n/a		
290	4.81	8.86	Weak	No, No	Strong	No, No		
1220	2.86	8.26	Small	n/a, No	Strong	No, n/a		
1222	2.95	9.38	Medium	n/a, No	Strong	No, n/a		
1227	4.53	9.91	Medium	No, No	Strong	No, n/a		
1241	3.04	8.65	Small	n/a, No	Small	No, n/a		
1265	2.84	9.30	Small	No, No	Strong	No, n/a		
1269	2.93	9.45	Small	No, No	Strong	No, n/a		
2645	5.07	7.95	Medium	n/a, No	Weak	No, n/a		
5004	6.72	12.36	Small	n/a, No	Strong	No, n/a		
5039	6.41	13.54	Weak	No, No	Strong	No, n/a	[O III] <sub>(4959+5007)</sub> , H <sub>α,β,δ,γ</sub> , [N II] <sub>(6583)</sub> , [S II] <sub>(6719+6730)</sub>	Emission lines observed only on the AAOmega spectrum
5042	8.65	12.26	Medium	No, No	Strong	No, No		Warm absorption lines observed with some C <sub>2</sub> features, but no CN
KDM 5651	8.96	12.75	Strong	No, No	Strong	No, No		
New Cold RCB candidates that need further monitoring								
136	4.83	9.66	Weak	n/a, n/a	Small	Em., n/a		
137	4.66	9.54	Small	n/a, n/a	Weak	Em., n/a	[N II] <sub>(6583)</sub>	
138	4.76	9.67	Small	n/a, n/a	Weak	No, n/a	[N II] <sub>(6583)</sub>	
150	4.67	9.14	Small	n/a, n/a	Weak	No, n/a		
164	3.41	8.36	Small	n/a, n/a	Small	No, n/a		
181	2.99	8.73	Medium	n/a, n/a	Weak	No, n/a		
194	2.94	7.57	Small	n/a, n/a	No	No, n/a	Na I D	
207	3.08	7.93	Small	n/a, n/a	n/a	No, n/a		
218	6.25	11.07	None	n/a, n/a	n/a	No, n/a		
223	1.25	7.27	Small	n/a, No	Strong	Em., n/a	Na I D	
225	3.25	7.95	Weak	n/a, n/a	n/a	No, n/a		
264	5.88	10.90	Small	n/a, n/a	Weak	No, n/a	Na I D	
274	1.03	6.33	Small	n/a, n/a	n/a	Em., n/a		2.3 m/WiFeS featureless spectrum
4117	2.33	7.64	None	n/a, n/a	Weak	No, n/a	Na I D	

the details of these atomic lines between 5500 and 9500 Å comparing synthetic spectra to the observed spectrum of the known Warm RCB star, UX Ant. Most of the lines observed at this resolution can be explained by the elements just mentioned, in particular, the strong C I absorption lines at 7112 Å and between 9050–9100 Å, the O I line at 7774 Å, and the Si II lines at

6345+6374 Å. Other weaker C I, N I, and O I lines are mostly blended with Fe I lines, but the resulting features remain clearly identifiable.

Using these indicators, we searched the ToI spectra presenting no sign of Paschen lines and no or only weak H<sub>α</sub> absorption. Thus, we identified 14 new Warm RCB stars. Their spectra are

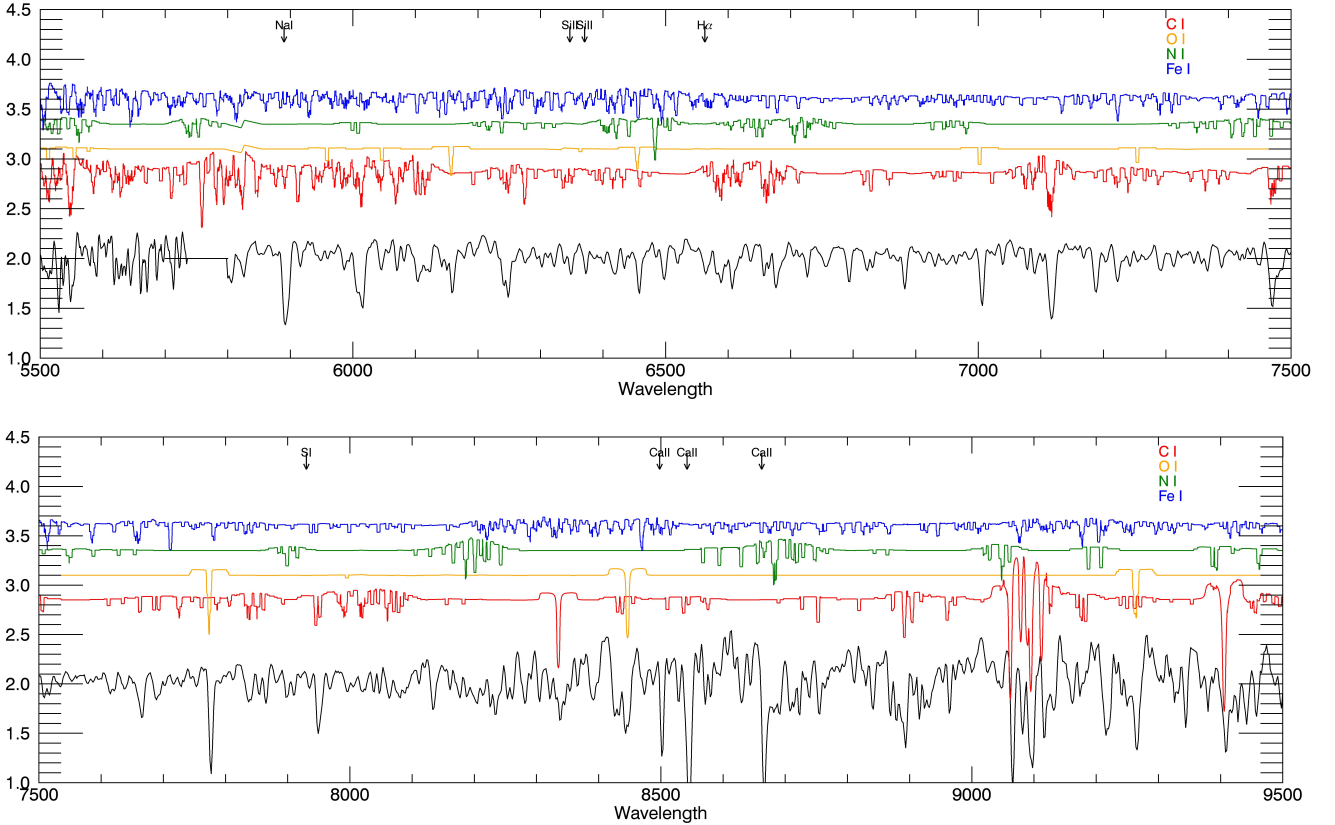


**Fig. 10.** Warm RCB star UX Ant (black) plotted with model stellar atmosphere spectra of C I (red), O I (yellow), N I (green), and Fe I (blue).

shown in Fig. 11, they look remarkably similar. The main differences we found are in the strengths of the O I and Si II lines (Table 7). ToI 5003 is the first Warm RCB star found in the Small Magellanic Cloud.

The principal difficulty in detecting new Warm RCB stars comes from similarities with RV Tauri stars. Indeed, these stars have similar photospheres, circumstellar shells, and  $T_{\text{eff}}$  to RCB stars, and therefore pass all the pre-selection criteria to be spectroscopically studied. Furthermore, they also show atomic absorption lines similar to Warm RCB stars, mainly the C I and Si II lines. However, RV Tauri star atmospheres are rich in hydrogen, and one can clearly detect the Paschen and  $H_{\alpha}$  absorption lines, and sometimes CH. Interestingly, to emphasise even more the similarity observed between both classes of stars, we found that some RV Tauri star light curves may present very rapid and large declines due to dust obscuration events that are similar to RCB stars. The main difference being the longer and larger amplitude of RV Tauri star photometric pulsations at maximum brightness. As an example, we present in Fig. 12 the light curve of WISE J175938.45–293321.8 (ToI 2571), an object whose brightness variation at maximum is similar to an RV Tauri star of RVb type with a period of about 500 days. On top of these variations, strong photometric declines can be seen, the last one being very large at JD  $\sim$  2455900 days.

On the same subject, we found that the star, OGLE-GC-RCB-2, was wrongly reported as an RCB star in Tisserand et al. (2011). Indeed, its identification as an RCB star was only based on its OGLE light curve as a sudden and large photometric decline was observed (see Fig. 5 in that article) but without any spectrum to support the claim. We later obtained a spectrum that shows all the features we have just indicated for an RV Tauri star. It stresses the need for spectroscopic follow-up to identify

new RCB stars. The light curve is a useful indicator but it is not sufficient.

ToI 1247 is a similar example. Its OGLE light curve shows multiple non-periodic declines very similar to RCB stars. It would have been classified as such after a classical dedicated search based only on its light curve, but the spectrum shows no classic Warm RCB star lines. It shows  $H_{\alpha}$  but no Paschen lines. We do not have a classification for this star. We will observe it again in case there is confusion between a classical H-rich main sequence star and a real RCB star that could have undergone a decline at the time of our observation.

Two new Warm RCB stars are listed in Table B.1 without any ToI identifier. They were followed up after extending our search just outside the colour cuts defined in Sect. 2.2.1. They are J174111.80–281955.3 and J174119.57–250621.2, located within 3 degrees of the Galactic centre. They did not pass the colour criteria on  $J - H$  versus  $H - K$  due to the very high reddening in that particular area of the sky.

With the detection of 14 new Warm RCB stars, we have reached a total of 45, representing nearly a third of the total number of RCB stars known (most of them being Cold). As an RCB star is supposedly evolving from a cold to a warm state before finishing its life as a heavy white dwarf, this ratio could indicate the relative time passed in both temperature regimes (Saio & Jeffery 2002; Montiel et al. 2018; Lauer et al. 2019).

#### 4.3. Third group: possible new RCB stars undergoing a dust obscuration event

When an RCB star undergoes a dust obscuration event, multiple emission lines appear in the spectrum, which evolve depending on the decline phase. A summary of these lines was detailed by

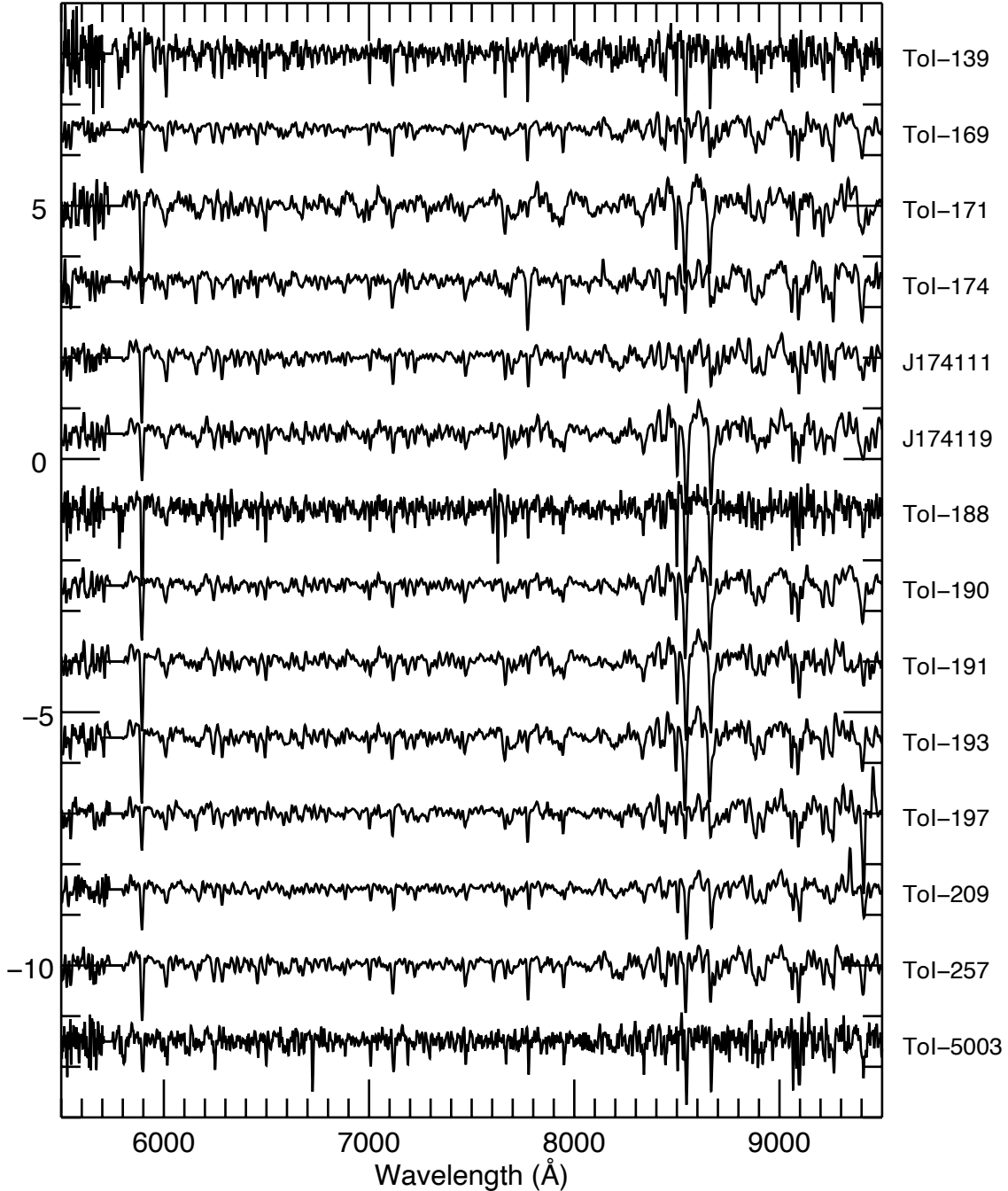


**Fig. 11.** Spectra of the newly discovered Warm RCB stars. From the top, the stars are ToI 139, ToI 169, ToI 171, ToI 174, WISE J174111.80–281955.3, WISE J174119.57–250621.2, ToI 188, ToI 190, ToI 191, ToI 193, ToI 197, ToI 209, ToI 257, and ToI 5003.

Clayton (1996) and Kameswara Rao et al. (2004). Early in the decline, many narrow emission lines blue-shifted from the stellar radial velocities (Spite & Spite 1979; Cottrell et al. 1990) are visible. A few weeks later and until the end of the decline phase, on top of a very reddened RCB star spectrum, one could see a few broad emission lines, the most common ones being Ca II H and K, and the Na I D lines. Only the Na I D line is detectable in the wavelength range of our optical spectra.

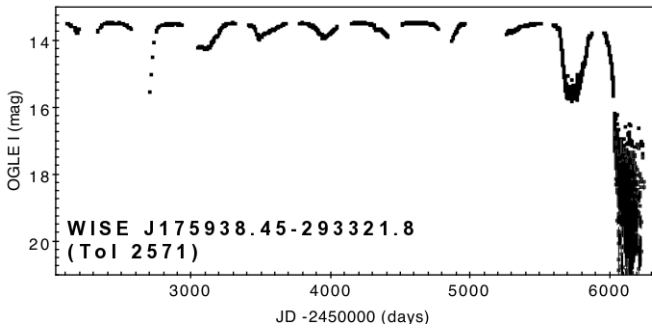
Detailed studies done at minimum light on three RCB stars, V854 Cen (Kameswara-Rao & Lambert 1993), UW Cen (Kameswara Rao et al. 2004), and R CrB (Kameswara Rao et al. 2006) show that one can also expect to observe broad emission lines for the following elements: [N II] (5755, 6548,

and 6583 Å in higher strength order), He I (5876 and 7065 Å), Ca II IR triplet, and [Ca II] (7291 and 7323 Å), but also, less commonly, [O I] (6300 and 6363 Å), some weaker lines, [S II] (6717 and 6731 Å) and K I (7664 and 7699 Å) lines, and the C<sub>2</sub> Swan bands. In the particular case of the less hydrogen-deficient V854 Cen RCB star, H<sub>α</sub> was also detected in emission (Lawson 1992). With that knowledge in hand, we searched our spectra for such features.

We searched for Na I D broad emission lines and found four members of the Cold group that show a red carbon spectrum with such emission. They are ToI 194, 223, 264, and 4117. For ToI 223, one can also observe weak H<sub>α</sub> in emission as well as [O I] at 6300 Å. No other broad emission lines were observed

**Table 7.** Spectroscopic analysis of new warm and hot RCB stars.

WISE All-Sky designation	WISE [12] mag	2MASS <i>K</i> mag	Ca II IR triplet strength	H $\alpha$ ?	Warm RCB abs. lines?	Comments
New Warm RCB stars						
139	5.43	9.60	Small	No	Yes with Si II	
169	5.54	9.66	Weak	small H $\alpha$	Yes with Strong Si II	
171	4.47	9.61	Strong	No	Yes with Si II	
174	6.86	9.70	Weak	small H $\alpha$	Yes with Strong Si II	
J174111–28	5.27	9.40	Small	No	Yes with Si II	
J174119–25	6.00	9.89	Medium	No	Yes with Si II	
188	3.99	8.30	Strong	No	Yes with Si II	
190	5.14	9.58	Strong	No	Yes	
191	4.32	8.63	Strong	No	Yes with Si II	
193	5.10	8.67	Strong	No	Yes with Si II	
197	3.19	7.36	Weak	No	Yes with Strong Si II	Possible weak CH feature
209	2.75	7.88	Medium	No	Yes with Si II	
257	5.21	10.14	Medium	small H $\alpha$	Yes with Strong Si II	
5003	8.62	12.81	Medium	No	Yes with Si II	
New Hot RCB star						
6005	5.55	13.42	None	Emission	No	Many emission lines including He I <sub>(5876+6678+7065)</sub> , O I <sub>(7774, Pcyg.)</sub> , C I <sub>(9050–9100)</sub> and C II


**Fig. 12.** OGLE light curve of WISE J175938.45–293321.8 (ToI 2571). This is an RVb type RV tauri star that is presenting some large photometric declines on top of periodic variations at maximum brightness.

for the other three. ToI 223 could be a similar RCB star to V854 Cen which is less hydrogen-deficient than typical RCB stars. In its spectrum, one can also detect clear C<sub>2</sub> features between 6000–6200 Å, some strong Ca II IR triplet absorption, but no detectable <sup>13</sup>C lines. These characteristics support the case that it is a member of the RCB class. ToI 4117, also named IZ Sgr, is part of the lowest priority group, #5, because of the classification given in the SIMBAD database as, surprisingly, a Mira M6 star (Houk 1967), but it would have been part of the first priority group otherwise. There has clearly been a misclassification as we observe some weak CN features in our reddened spectra. Its light curve was also already selected by Tisserand et al. (2013) in their search for RCB stars in the ASAS database because two rapid and sudden photometric declines were observed. This target is therefore similar to ToI 218 discussed in Sect. 4.1.2 and a spectrum near maximum brightness is needed for a full confirmation of its nature. The reddened spectra of ToI 194 and 264 show clear CN features observed above 6900 Å, but no clear C<sub>2</sub> features in the interesting wavelength range as the signal level was weak and noisy. We consider all four targets as good Cold RCB candidates.

We also looked for spectra with broad emission lines from the other elements, mainly ToI that had [N II] (6583) in emission. This is the case of ToI 138 which we already classified as an RCB star in our group #1 Cold star sample analysis. No other lines are, however, observed, Na I D being in absorption. We found another interesting target, ToI 137, having [N II] (6548 and 6583 Å) in emission, but also He I (7065) and split emission lines of [O I] (6300) and of a weak H $\alpha$  suggesting a symmetric structure. Its reddened spectrum also shows some CN features in absorption after 6900 Å and some weak Ca II IR triplet absorption. Again ToI 137 could be a less hydrogen-deficient RCB. We consider it also as a Cold RCB candidate. All other spectra presenting [N II] in emission also show strong H $\alpha$  emission lines without an underlying red carbon spectrum, so we did not study them further.

Interestingly, we obtained a second spectrum of ToI 5039, a target that we already listed as a new cool Magellanic RCB star in the related section above, using the AAT/AAOmega spectrograph. The spectrum was observed on 2010-10-29 which corresponds to a moment of the deepest minimum as indicated by its OGLE-IV-RCOM light curve ( $I \geq 20.8$  mag). We observed some strong broad emission lines with the redshift expected for the LMC distance: [O III] (4959+5007 Å), [N II] (6583 Å), [S II] (6719+6730 Å), and also strong emission in the Balmer series ( $\alpha, \beta, \delta$ , and  $\gamma$ ). No obvious sign of hydrogen was observed in its spectrum taken closer to maximum brightness with the 2.3 m/WiFeS a year earlier (on 2009-11-27). ToI 5039 could also be like the less hydrogen-deficient V854 Cen.

In the extreme cases of high obscuration, the RCB star photosphere disappears from the spectrum and only the featureless spectrum of the circumstellar shell remains visible (García-Hernández et al. 2011). This is what was observed with ToI 274. Its spectrum (obtained the 2013-08-18 with the 2.3 m/WiFeS spectrograph) is of a very cool featureless blackbody. Only a weak and broad Na I D emission line is detectable. A later observation obtained with the automatic Liverpool telescope revealed a reddened spectrum with some CN features

above 6900 Å, but without any C<sub>2</sub> band-heads. We also note a weak and broad H<sub>α</sub> emission line. It was most certainly taken during a brighter phase. Further spectroscopic follow-up is needed on this particular ToI.

We consider ToI 274 as an RCB candidate as well as the other five ToI listed above. Their spectra show emission lines expected for RCB stars in decline but we need observations at maximum brightness to confirm their nature. ToI 223 and 4117 are the strongest candidates.

Recently Oostrum et al. (2018) reported an unidentified feature, located at 8692 Å, observed on the spectra of few RCB stars. We looked for such broad emission in our mid-resolution spectra and found that only one of our Cold RCB star candidates, ToI 164, showed a feature at that wavelength.

#### 4.4. Fourth group: Hot RCB stars

Among the rare group of RCB stars, there exists an even rarer subgroup with only four members known so far: MV Sgr, V348 Sgr, DY Cen, and HV 2671 (De Marco et al. 2002). They are the Hot RCB stars with  $T_{\text{eff}}$  between 15 000 and 20 000 K. In the context of the double degenerate merger scenario, they would represent the last phase of an RCB star evolution, where an RCB star evolves from Cold to Warm and then to Hot, while the atmosphere gets smaller and bluer. Such an evolution is supported by the long-term photometric analysis of known Hot RCB stars (De Marco et al. 2002; Schaefer 2016). The evolution to the blue is expected to continue and the Hot RCB stars would then become extreme helium stars (Jeffery 2008a,b; Lauer et al. 2019).

The spectra of Hot RCB stars show a hot blackbody continuum with many emission lines, in particular, C II and He I (Leuenhagen et al. 1994; De Marco et al. 2002). Some low-resolution optical spectra of three Hot RCB stars are also presented by Tisserand et al. (2013, Fig.16). We found that one of our targets, ToI 6005, presents a similar spectrum. It is shown in Fig. 13 with a spectrum of V348 Sgr for direct comparison. We consider it as a new Magellanic Hot RCB star. Along with many C II emission lines, are He I (5876, 6678 and 7065 Å), O I (7774 Å) and weak H<sub>α</sub> as seen in V348 Sgr. A detailed description of these lines is given in Dahari & Osterbrock (1984) who discussed the spectra of V348 Sgr observed at various epochs. Furthermore, the OGLE surveys have observed a light curve for ToI 6005 that clearly shows two large and rapid declines before a recovery to a brighter phase (the overall variation is >5 mag in I band).

## 5. Status of previously proposed RCB candidates

Here, we discuss the status of strong RCB candidates accumulated during the years and for many of which we have update, and the status of candidates reported by four articles or research notes (Soszyński et al. 2009; Lee 2015; Nikzat & Catelan 2016; Shields et al. 2019) published lately.

### 5.1. Strong candidates

Ten strong candidate RCB stars are listed at the end of Table A.1, some because of photometric declines observed in their light curves but without any spectroscopic confirmation, others because they show interesting featureless mid-infrared spectra but have no other information yet to support their classification as RCB stars.

Interestingly, four of them were selected in the present analysis, namely, GLIMPSE-RCB-Cand-1, GLIMPSE-RCB-Cand-2, MSX-LMC-1795 and EROS2-SMC-RCB-4. They are listed in our catalogue as priority Group #1 targets with respectively the following Ids: 188, 204, 5039 and 5005. We succeeded in getting spectra for three of them and we can now confirm them as bona fide RCB stars. GLIMPSE-RCB-Cand-1 (i.e. ToI 188) and GLIMPSE-RCB-Cand-2 (i.e. ToI 204) were the first stars selected after a series of IR colour criteria using the 2MASS and *Spitzer*/GLIMPSE magnitudes (Tisserand et al. 2011), and for which a spectroscopic follow-up has shown interesting carbon features and very red continua, being located at less than 3° from the Galactic plane. There were no light curves available at the time. We have classified these two stars as Warm and Cold RCB stars respectively, as they have satisfied all the criteria defined in each category. Furthermore, we now have a light curve available for ToI 188, as it was observed by the OGLE-IV survey. It shows a characteristic sudden 8 mag decline that occurred in 2015. The third known candidate that we have now confirmed is MSX-LMC-1795 (i.e. ToI 5039) located in the Large Magellanic Cloud. It was first reported by Matsuura et al. (2014) as a potential RCB star due to its featureless mid-IR spectrum and the suspicion got stronger with its OGLE light curves. Indeed it showed a 4 mag variation during the OGLE III monitoring (Soszyński et al. 2009, see object OGLE-LMC-RCB-21), and six declines with maxima getting brighter each time during the last OGLE-IV phase<sup>4</sup>. We have now succeeded in getting a spectrum and it has been classified as a Cold RCB star.

We have not yet succeeded in obtaining a spectrum for the fourth remaining RCB candidate, EROS2-SMC-RCB-4 (i.e. ToI 5005). This star is an interesting case as it has remained faint for the past 19 years. Indeed, after a short 4.5 mag decline that occurred in 1998 as reported by the EROS2 survey in Tisserand et al. (2009), the OGLE survey data have not reported any variations<sup>5</sup>. EROS2-SMC-RCB-4 has remained highly enshrouded, indicating a continuous production of dust in the line of sight. We also suspect that it did not reach its maximum brightness during the short recovery phase in 1998. If confirmed as an RCB star, EROS2-SMC-RCB-4 could be the first of a population of very cold, highly enshrouded RCB stars. Its brightness needs to be monitored to trigger a spectroscopic alert. It was reported by Ruffle et al. (2015) to present a mid-IR featureless spectrum which strongly supports its classification as an RCB star. Long duration decline phases is not uncommon in RCB stars. R CrB itself recovered recently from a 10 year decline, and V854 Cen spent several decades in a deep decline in the early 20th century (McNaught 1986).

Of the six remaining RCB star candidates that did not pass the selection criteria defined in Sect. 2, three of them, KDM 5651, OGLE-GC-RCB-Cand-1 and [RP2006] 1631, did not pass the criteria imposed on the shell colours (detailed explanation are given in Sect. 2, cut #2). We obtained a spectrum of KDM 5651 and OGLE-GC-RCB-Cand-1. We confirm KDM 5651 as a bona fide Cold RCB star. The spectrum of OGLE-GC-RCB-Cand-1 is highly reddened, almost featureless, with only some weak Ca II IR triplet lines detected. It certainly corresponds to the bluest part of the dust shell as we observed this star during a decline phase. Indeed, at the time of the observation (epoch:

<sup>4</sup> <http://ogle.astrouw.edu.pl/ogle4/rcom/ogle-lmc-rcb-21.html>

<sup>5</sup> RCOM OGLE III: <http://ogle.astrouw.edu.pl/ogle3/rcom/eros2-smc-rcb-4.html> and RCOM OGLE-IV: <http://ogle.astrouw.edu.pl/ogle4/rcom/eros2-smc-rcb-4.html>

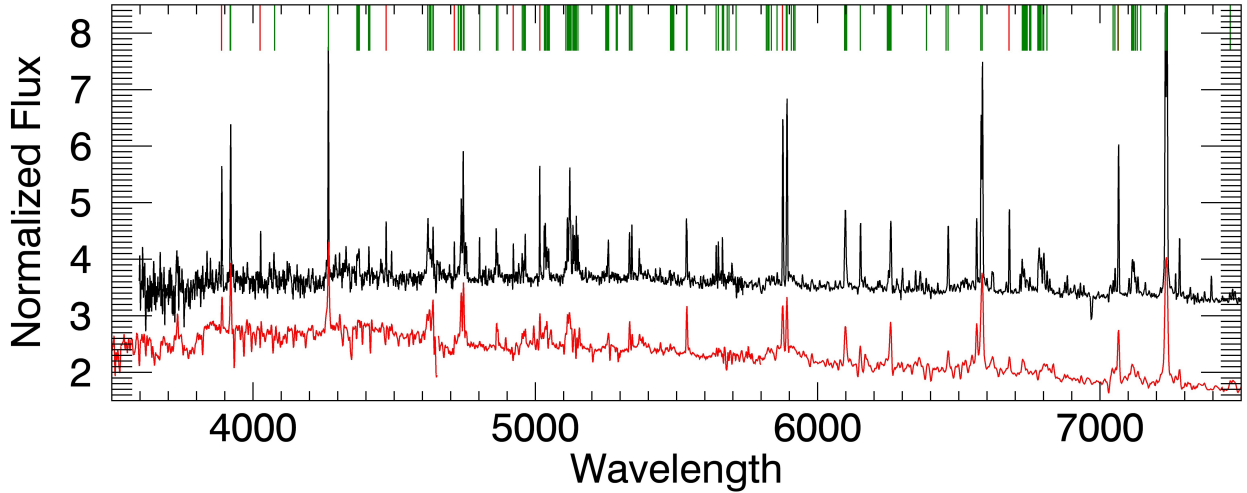


**Fig. 13.** Spectrum of the new LMC Hot RCB star (black), WISE J053745.70-635330.8 or ToI 6005, plotted with that of another Hot RCB star, V348 Sgr (red), for comparison (De Marco et al. 2002). The emission lines are mostly C II (green lines) and He I (red lines). The ordinate is arbitrary.

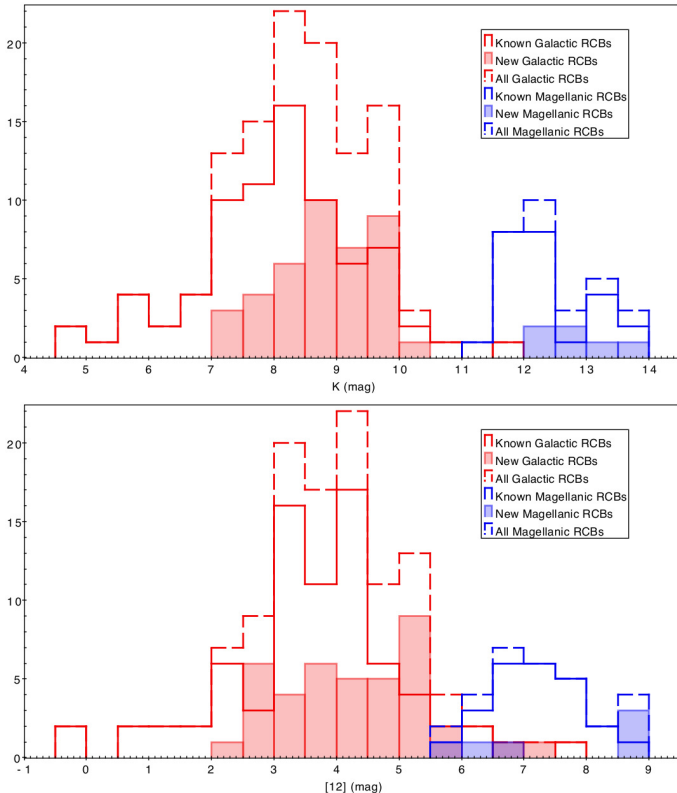


**Fig. 14.** Distributions of magnitude in the  $K$  (top) and  $[12]$  (bottom) bands for all previously known and newly discovered RCB stars.

2010-07-16,  $I \sim 15.43$  mag), its OGLE-IV light curve shows that it was 1.2 mag fainter than its maximum magnitude. Most of the signal received was therefore from the circumstellar dust shell. We will wait for a brighter phase to observe it again. It is located only a few degrees from the Galactic centre at  $(l, b) \sim (0^\circ 14, -1^\circ 6)$ , and therefore one expects a high interstellar extinction. From its light curve, presented in Tisserand et al. (2011), and its position in the  $J - H$  versus  $H - K$  diagram near the giant carbon stars locus, OGLE-GC-RCB-Cand-1 could potentially be a DY Per type star. DY Per type stars are potentially the cooler counterparts of RCB

stars (see Tisserand et al. 2013, Sect. 3.4 and Bhowmick et al. 2018). We still did not succeed in observing [RP2006] 1631 spectroscopically. A featureless mid-IR spectrum was presented by Woods et al. (2011). That is typical of RCB stars circumstellar shell.

The eighth RCB star candidate, EROS2-LMC-RCB-7, was found to have similar  $K$  brightness and  $J - K$  colour to Magellanic extreme AGB stars (see Fig. 3). Its light curve, presented in Tisserand et al. (2009, Fig. 10 top-left), shows only a weak variation typical of a highly enshrouded object. We think it is not an RCB star.

The last two candidates, EROS2-LMC-RCB-8 and OGLE-GC-RCB-Cand-2, have shown similar IR photometric colour to the known RCB stars, EROS2-CG-RCB-12 and MACHO 308.38099.66 (see Fig. 2 right side). However, these four stars are located at the position where the AGB-star locus lies, outside the main selection area chosen for RCB stars. Their real nature is therefore suspicious, but a reddening effect during a photometric decline event could explain such position. That is the case for the two known RCB stars and OGLE-GC-RCB-Cand-2 whose 2MASS epochs were taken during a decline phase, but not for EROS2-LMC-RCB-8, that was observed during a bright phase. The light curves of EROS2-LMC-RCB-8, OGLE-GC-RCB-Cand-2 and EROS2-CG-RCB-12 are presented respectively in Tisserand et al. (2009, Fig. 10), (Tisserand et al. 2011, Fig. 5) and Tisserand et al. (2008, Fig. 9). Some sudden and large declines ( $>3$  mag) were observed on top of large amplitude periodic oscillations ( $\sim 1.5$  mag) at maximum brightness for these three objects. These declines triggered their classification as possible RCB stars, however the large oscillations are not seen in any other RCB stars. The typical RCB star amplitude is between  $\sim 0.1$ – $0.3$  mag (Lawson & Cottrell 1997). Furthermore, the light curve of OGLE-GC-RCB-Cand-2 shows only a slow recovery phase, no fast photometric decline has ever been observed, and, in regards to EROS2-LMC-RCB-8, it is brighter in  $K$  than any other Magellanic RCB stars and is located just near the main distribution of AGB stars in the  $J$  versus  $J - K$  diagram (see Fig. 3). However, they all have been observed spectroscopically and are all cold carbon stars with no obvious hydrogen features. EROS2-CG-RCB-12 even shows the Ca II IR triplet in emission, as seen in RCB stars undergoing photometric declines. More investigations will be needed to

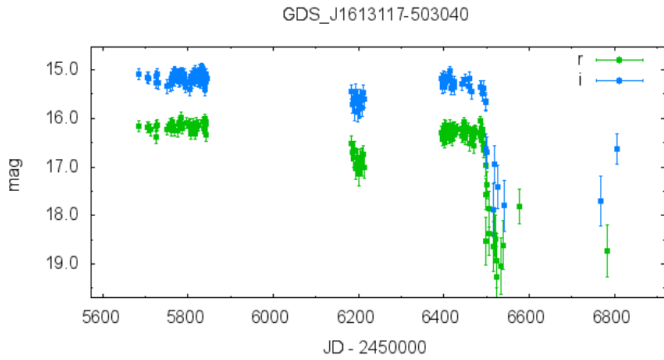


**Fig. 15.** Light curve of GDS J1613117–503040 from the Bochum survey (Hackstein et al. 2015). A fast photometric decline of 3 mag is observable around JD~2456500 days in both the  $r$  and  $i$  bands. This star is surrounded by two distinct circumstellar dust shells and was therefore not selected by our IR photometric selection criteria. We consider it as an RCB candidate that needs a spectroscopic follow-up for confirmation.

understand if these stars are very cold RCB stars or more classical carbon Mira type stars undergoing dust production events similar to RCB stars.

The light curve of MACHO-308.38099.66 (see Zaniewski et al. 2005, Fig. 1b) does not show any large amplitude oscillations. Two decline episodes of two magnitudes in the visible were reported by the MACHO survey, while the star presented small  $\sim 0.1$  mag pulsations at maximum brightness. It was observed by 2MASS during the second decline phase and is located at Galactic coordinates  $(+10.3, -2.9)$  where an interstellar extinction of  $A_V \sim 3.0$  mag (Schlafly & Finkbeiner 2011) is expected. MACHO-308.38099.66 is very likely an RCB surrounded by a hot ( $>800$  K) circumstellar shell and is located at the AGB star locus because of reddening effects.

Finally, we add as a new RCB star candidate, WISE J161311.79–503040.2, also known as GDS\_J1613117–503040. We list it as such because of the spectacular brightness declines of 3 mag observed in its Bochum survey light curve (see Fig. 15). The SED of this star shows that it is surrounded by two thick circumstellar shells, as are the known RCB stars MV Sgr, DY Cen, and MACHO-11.8632.2507, and was therefore not selected by our criteria. We need a spectroscopic confirmation of its real nature. Similarly to OGLE-GC-RCB-Cand-1, one can expect a high extinction along the line of sight to this star as it is located near the Galactic plane at  $(l, b) \sim (332^\circ, 3, 0^\circ)$ . The presence of two dust shells around RCB stars seems to be common (Montiel et al. 2018).

## 5.2. Candidates recently published in the literature

### 5.2.1. Candidates from Soszyński et al. (2009)

Soszyński et al. (2009) went through their OGLE-III catalogue of LPV stars that show unusual IR characteristics and selected the ones that exhibit irregular fading episodes. They found six candidates towards the LMC, namely OGLE-LMC-RCB-03, -09, -15, -16, -20 and -21. In all cases except one, OGLE-LMC-RCB-21, the maximum variations observed were small (between 0.3 and 0.8 mag) and for the first four candidates, the fadings were not typical of RCB stars. None of these first four candidates are present in our list of targets of interest, because OGLE-LMC-RCB-09 was not catalogued in the WISE AllSky or even ALLWISE databases, and because none of the other three had WISE colours that satisfied the second selection criterion (see cut

#2 in Sect. 2.2.1). We had followed them up spectroscopically nevertheless and found that OGLE-LMC-RCB-03 and OGLE-LMC-RCB-15 present spectra of F stars with typical Ca H and K absorption lines and Balmer lines, while the other two, OGLE-LMC-RCB-09 and OGLE-LMC-RCB-16, show spectra of Be stars with Balmer, Paschen and He I lines in emission. Concerning the last two candidates reported, OGLE-LMC-RCB-20 and -21, we already mentioned them in this present article as they are the now confirmed RCB stars, respectively KDM 5651 and WISE J054221.91-690259.3 (ToI 5039).

### 5.2.2. Candidates from Lee (2015)

Lee (2015) used the IR selection criteria, that were developed by Tisserand (2012) to retrieve a list of objects from the WISE ALL-Sky database. They cross-matched all of the selected objects with the catalogue of the Catalina survey, which has monitored the sky on both sides of the Galactic plane ( $|b| > 15$  deg) for over 8 years, to find those that have varied by more than 1 magnitude during that period. They found 26 interesting objects, five of them being already known RCB stars. In the second stage of their study, from the analysis of the Catalina light curves and the objects' SEDs, they reported that only three of the 21 remaining objects could be considered as RCB candidates. J194218.38-203247.6 shows seven large non-periodic photometric variations and a reported flat SED between 1 and  $10 \mu\text{m}$ . This object was also selected by our analysis (ToI 290), and, after a spectroscopic follow-up, we classified it as a new RCB star (see Table B.1). J062741.84-681016.2 and J160701.19-143446.7 show similar long term increases in brightness (resp. 2 mag over  $\sim 500$  days, and 3 mag over  $\sim 1500$  days) typical of RCB stars during their phase of photometric recovery after a large decline. However, the authors are less optimistic with these last two objects. The former presents a single-component SED of a cold black-body and is therefore most certainly a N-type AGB star. The SED of the latter star has little optical photometry to pinpoint its overall shape. We have followed-up J160701.19-143446.7 spectroscopically as it was also selected in the present analysis, ToI 1189, and we found it to be a cool carbon-rich AGB star presenting H-alpha emission.

We cross-matched their additional 21 objects with our list of ToI and found eight objects are in common. That is not surprising, as the IR selection criteria used in both cases are quite similar. The criteria developed in the present study being more restrictive than those presented in Tisserand (2012). These objects are: J023405.26+373352.8 (ToI 1014), J063856.03+5429 40.4 (ToI 33), J070137.95-412816.5 (ToI 1042), J085725.83+ 172052.0 (ToI 1079), J160701.19-143446.7 (ToI 1189), J164 327.28-141200.2 (ToI 1199), J194218.38-203247.6 (ToI 290) and J222704.54-165948.5 (ToI 323). Most of them belong to the priority #2 group (i.e. ToI Id between 1000 and 1999), where the main background expected is very cold AGB stars ( $J - K > 3.5$  mag). Their Catalina light curves are also not convincing as many large periodic variation are seen. The only two stars we have already followed-up spectroscopically during our survey are ToI 290 and ToI 1189 (see our result in the previous paragraph).

### 5.2.3. Candidates from Nikzat & Catelan (2016)

Some three RCB star candidates and 63 DY Per type candidates were listed by Nikzat & Catelan (2016) based only on their OGLE light curves. Unfortunately, the IR  $J - H$  versus  $H - K$  that could have been simply used to differentiate between

**Table 8.** Status of candidates from Shields et al. (2019) in our study.

ASASSN-V designation	ToI Id ?	Status from our study
Their Table 1 – “Candidates RCB stars”		
J053745.71–635330.9	6005	Confirmed RCB star
J053213.93+340601.4	23	
J173819.81–203632.2	1227	Confirmed RCB star
J173737.08–072828.2	1225	
J174257.20–362052.1	184	Confirmed RCB star
J190309.89–302037.0	264	Strong RCB candidate
J170737.02–314812.5		
J175031.71–233945.7	191	Confirmed RCB star
J044531.02–683431.3		
J004822.94–734104.6		
Their Table 1 – “Large amplitude candidates”		
J174317.53–182402.5	185	
J170552.81–163416.6	1213	
Their Table 1 – “DY Per stars candidates”		
J191243.07+055313.1	274	Strong RCB candidate
J175526.28–214214.1	2554	RV Tauri? Warm H-rich star
J202300.80+431111.5	302	
Their Table 2 – “RCB Candidates discovered outside our search”		
J161156.22–575527.2	124	Confirmed RCB star
J043259.32+415854.0		
J201504.29+462719.9		
Their Table 2 – “DY Per candidates”		
J175700.51–213934.5	199	RV Tauri? Warm H-rich star
Their Table 3 – “Weak RCB Candidates”		
J195525.11+015601.6		
J075155.45–331057.2		
J185316.37–271352.7	2801	M star
J174445.73–362232.3	187	
J174328.51–375029.1	186	Confirmed RCB star
J163750.78–644140.5	2317	M star
J174731.77–444501.4		
J173257.95–180435.6		
J211119.06+473847.7		
J054551.71+350300.0	2030	
J172216.67–281656.9	2409	
J174825.52–324240.5		
J160407.52–580250.6		
J181154.33–241827.3		
J054424.84–655814.2	5041	
J181214.33–252406.5	2642	Hot H-rich star

DY Per type stars and RCB stars, as in Morgan et al. (2003) and Tisserand et al. (2009), was not applied in that search. We cross-matched their list with the 2MASS and the WISE AllSky databases. We found that the first two RCB candidates listed, OGLE-SMC-LPV-01019 and OGLE-SMC-LPV-06216, should in fact be listed as good DY Per type candidates. Indeed, their IR characteristics are similar to those expected and their OGLE light curves are very similar to other DY Per type stars (Alcock et al. 2001; Tisserand et al. 2004, 2009). Furthermore, they were both previously catalogued as carbon stars in the SMC surveys (Morgan & Hatzidimitriou 1995; Rebeiro et al. 1993). They are named, respectively, [MH95] 219 and RAW 380. The reason to list the third and last object, OGLE-SMC-LPV-17611, as an RCB candidate, is only based on a visual similarity observed by the authors of its OGLE light curve with the one of the strong

RCB candidates, MSX-SMC-014. However, we note that the light curve of MSX-SMC-014 shows some brightness increase and decline back to a faint background level (that is expected for star with a high rate of dust formation) while OGLE-SMC-LPV-17611 shows only two magnitudes of variability at a low median brightness level ( $I \sim 20$  mag). We checked the IR characteristics of OGLE-SMC-LPV-17611 and found that while it shows an excess in the  $J - H$  versus  $H - K$  diagram as expected for RCB stars, we would not have selected it in the mid-IR, as it did not pass the selection criteria #2 (closely) and #3 (more convincingly). That star need nevertheless a spectroscopic confirmation. Concerning the other 63 DY Per type candidates, we found that many of them do not have the IR characteristics expected for these stars. Two of them are listed in our catalogue of Targets of Interest for our search of RCB stars, namely, OGLE-SMC-LPV-16850 (ToI 6002) and OGLE-SMC-LPV-17267 (ToI 9006). We have not yet observed these stars spectroscopically. However, their OGLE light curves are not convincing as long period variabilities are observed.

#### 5.2.4. Candidates from Shields et al. (2019)

The authors published a list of 19 RCB and DY Per type candidates that were selected based on the photometric variability observed in the ASAS-SN survey (Shappee et al. 2014), and added another 16 weaker candidates. To do so, they started from a list of stars with similar IR characteristic than RCB stars. These objects are the 1602 targets listed by Tisserand (2012) and 2006 new ones that they selected over the entire sky with the WISE ALLWISE database using the original idea of selecting objects after fitting their SED to each of the known RCB stars. They kept the ones with quasi-identical SED, extinction and distance corrected, to any of the known RCB stars they used.

Many of the candidates selected are in fact also listed in our catalogue of targets of interest, that is, 14 out of their 19 strong candidates, and a further eight out of their 16 weaker candidates. We list the ToI id for each of the candidates we have in common in Table 8. We also give a classification based on our spectroscopic follow-up observations, if such data exist. That was the case for 13 objects out of the 22 candidates we have in common. In summary, six of them are also ToI that we have now confirmed as new RCB stars and two others are ToI that we have listed as strong RCB candidates (see Table B.1). We also report that five objects are not RCB stars, as two are Mira type objects, two others are potentially RV Tauri stars, and one shows an H-rich emission spectrum.

## 6. Results and discussion

For the 488 WISE ToI that we have followed up spectroscopically, there is a success rate of nearly 10% of bona fide new RCB stars. This rate is even higher when we only consider the priority group #1 targets. In that subgroup, the success rate rises to ~25% with about 40% of those targets followed up. The success rate for priority group #2 is slightly lower, ~19%, while only ~10% of this group’s targets were followed up. For group #3, we found only one new RCB star among the 256 ToI (i.e. a quarter of all group #3 ToI) observed. Half of our observational efforts were made on that group as it contains many bright targets. We found that most objects in this group are Mira and RV Tauri stars, but it should also contain some rare RCB stars that possess very thick circumstellar shells. Furthermore, we have light-curve information for a further 199 ToI (mostly from priority group #3) that show clear photometric oscillations similar to Miras or RV Tauri

stars. Overall, we have obtained a conclusive definition of the nature of 687 ToI, which is almost a third of all ToI listed. (It corresponds to  $\sim 45\%$ ,  $\sim 12\%$ ,  $\sim 36\%$ ,  $\sim 6\%$ , and  $\sim 37\%$  of the targets from the priority groups #1 to #5 respectively; see Table 3).

### 6.1. Galactic distribution and magnitudes of new RCB stars

As expected, the luminosities of the newly found RCB stars are on the fainter end compared to the known stars. This is illustrated in Fig. 14 showing the magnitude distribution in  $K$  and  $[12]$  bands for both Galactic and Magellanic RCB stars. However, it is worth noting that two Cold RCB candidates, ToI 223 and 274, have bright circumstellar dust shells with  $[12] \sim 1.2$  and  $\sim 1.0$  mag, respectively (see Table 6). If confirmed as RCB stars, they would be respectively the fifth and sixth brightest RCB stars in the  $[12]$  band. Furthermore with an interstellar extinction of  $A_V \sim 8$  mag (Schlafly & Finkbeiner 2011) and an apparent  $K$  magnitude of 6.3 mag, ToI 274 could be one of the ten brightest Galactic RCB stars.

Figure 16 presents the spatial distribution of all ToI and of the 488 targets already observed spectroscopically. We found new RCB stars on both sides of the Galactic plane, and from a simple first distance estimate based on their  $K$  band luminosity, most of them are located beyond the Galactic centre. Our observational effort was concentrated mostly between the Galactic longitude range  $[-60^\circ, +45^\circ]$  as we used telescope facilities in the southern hemisphere. The distribution of the interesting ToI in the priority categories #1 and #2, that remain to be observed (see Fig. 16, top-right), suggests that future observations will have to focus outside the Galactic Bulge and mostly along the Galactic disc.

### 6.2. How many Galactic RCB stars exist out there?

Taking the results reported here into consideration, we can make an initial estimate of the total number of RCB stars in our Galaxy. A total of 77 Galactic RCB stars had been identified before this first dedicated all-sky search (Tisserand et al. 2013). This work identifies 40 new RCB stars, increasing the total to 117 Galactic RCB stars. So far only a few of the ToI listed in priority group #4 have been followed up because most of them are faint highly enshrouded stars that require observations with 4 m-class telescopes. So if we choose an optimistic rate of discovery of 20% for this group, corresponding to about 50 new RCB stars, and similarly choose the favourable scenario that 20 new RCB stars can be discovered in both priority groups #3 and #5, we would reach a potential of about 220 new discoveries within the remaining list of ToI, assuming we add 50 and 77 potential new RCB stars from respectively the categories #1 and #2 groups, simply using the rate of discovery obtained so far. When corrected for the 85% detection efficiency of the ToI photometric selection process, we estimate that in this favourable scenario there could be as many as about 380 RCB stars existing in the Galaxy  $(77 + (220 + 40) / 0.85)$ .

This is a rough estimate, and, of course, our all-sky search has biases as it was optimized using the known RCB stars. We summarize briefly the selection biases as we know them. A more detailed discussion can be found in Sect. 2.3. Firstly, we do not know much about the highly enshrouded RCB stars, such as EROS2-SMC-RCB-4 and MSX-SMC-014. They have remained faint most of the time during the past 20 years and have been found to be surrounded by a thick dust shell presenting featureless mid-IR spectra (Kraemer et al. 2005; Ruffe et al. 2015). They are members of priority group #4, for which we assumed an optimistic discovery rate of 20%. Secondly, our search does

not target RCB stars that possess multiple bright dust shells (we know of three such RCB stars so far); and also RCB stars with either a very thin dust shell or no shell at all, like the HdC stars, will be missed. For the first two sets of stars, we have taken them into account via our detection efficiency, but their numbers could be underestimated. For the remaining group, the HdC stars, only five are known so far and considering that no dedicated deep all-sky searches were ever made to find more of them, we need to compare that number to the quantity of known bright Galactic RCB stars before the recent discoveries made using light curve surveys. We estimate there could exist up to one HdC star for every six RCB stars, which would thus correspond to a total of about 60 HdC stars in the Galaxy. Thirdly, our spectroscopic follow-up has mostly targeted ToI located within 60 degrees of the Galactic centre (see Fig. 16) and the external disc region of the Galaxy was not covered. However, RCB stars seem to follow an old-disc spatial distribution and should be found in higher numbers in the central area of the Galaxy. This observational bias would support our optimistic conservative approach in the estimate of the total number of Galactic RCB stars as a lower rate of discovery is expected at higher Galactic longitude. Finally, we know that the detection efficiency of our all-sky ToI selection drops within a few degrees of the Galactic centre and along the Galactic plane at low Galactic latitude due to high interstellar extinction. Targeted surveys found many RCB stars located within the Galactic bulge, but still outside the high extinction sky areas (Zaniewski et al. 2005; Tisserand et al. 2008). This could indicate that tens of new RCB stars potentially lie within the most highly crowded and reddened parts of the Galaxy.

Overall, we can confidently say from this first dedicated survey for RCB stars that it is unlikely that there are more than 500 HdC stars in the Galaxy, and that it is likely the population is somewhere between 300 and 500. These estimates are also consistent between the Galaxy and the Magellanic Clouds. Indeed, 30 RCB stars are now known in the Magellanic Clouds as we have added five in this study after the spectroscopic follow-up of 28 Magellanic ToI. With 86 Magellanic ToI remaining to be observed, mostly faint ones, we can estimate, in an optimistic scenario using a similar discovery rate, that about 20 Magellanic RCB stars are yet to be discovered. If the number of RCB stars scales with galaxy mass, the number we extrapolate in the Galaxy would then be  $\sim 550$  RCB stars  $(11 \times (30 + 20))$ .

This result is in excellent agreement with theoretical estimates made from population synthesis via the double-degenerate channel. Indeed, with a He-CO white dwarfs merger birthrate ranging between  $\sim 10^{-3}$  and  $\sim 5 \times 10^{-3}$  per year (Nelemans et al. 2001; Ruiter et al. 2009; Karakas et al. 2015) and an RCB phase lifetime of about  $10^5$  years, as predicted by theoretical evolution models (Saio & Jeffery 2002; Lauer et al. 2019), the expected theoretical number of Galactic RCB stars formed via the double-degenerate channel ranges between 100 and 500.

As discussed in the Introduction, another scenario, the final helium shell flash, has also been suggested as a channel for the formation of RCB stars. If a fraction of Galactic RCB stars are indeed formed through this scenario, our estimate of the total number of Galactic RCB stars is in fact the sum of RCB stars formed by both channels. The overabundance of  $^{18}\text{O}$  and  $^{19}\text{F}$ , and the large  $^{12}\text{C}/^{13}\text{C}$  ratios seen in most RCB stars are a natural product of the WD merger channel, but are not expected from a final flash (Clayton 2012; Lauer et al. 2019). However, there are a small number of RCB stars which differ significantly from the majority characteristics. These include stars with particularly extreme values of Si/Fe and S/Fe, and those with measurable  $^{13}\text{C}$ , and Li, that may be more easily explained by the final-flash

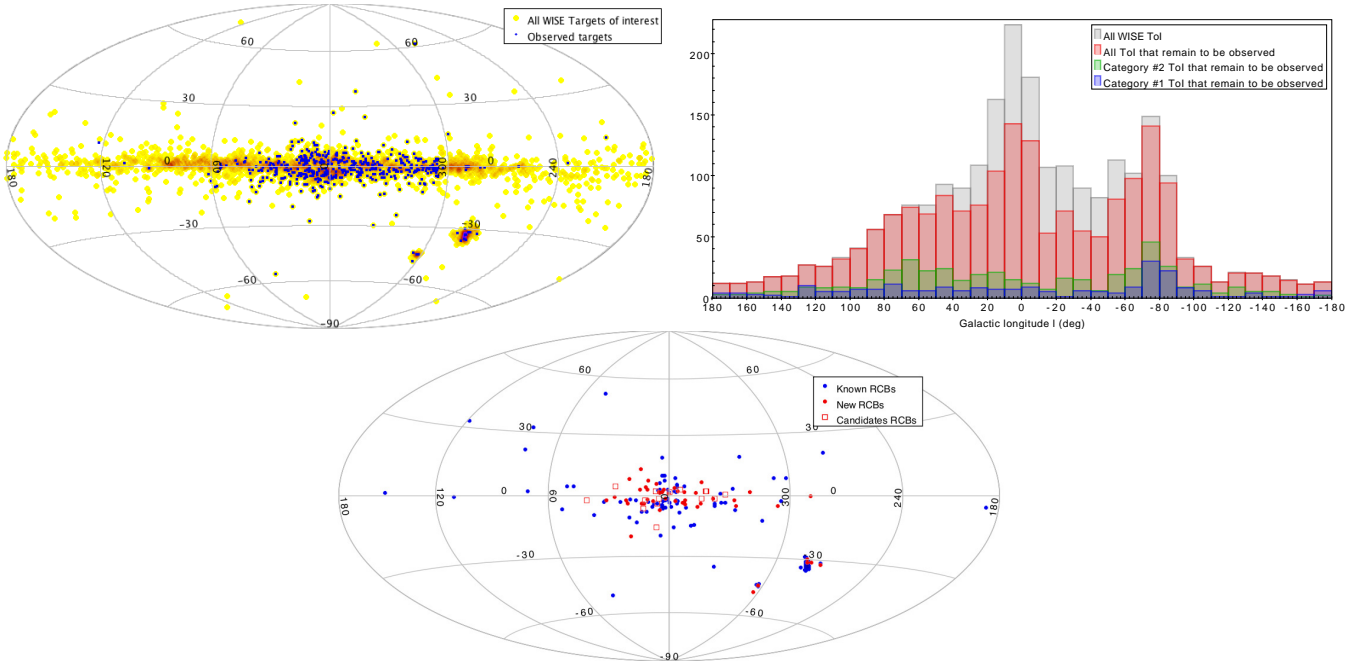


**Fig. 16.** Spatial distribution in Galactic coordinates of all selected targets of interest, overlaid with the ones already followed-up spectroscopically (*top left*). Distribution of all known and candidate RCB stars (*bottom*). Distribution in Galactic longitude of all ToI with the ones already observed and the remaining ones (*top right*).

channel (Asplund et al. 2000; Clayton 2012). However, Li production through the Cameron-Fowler mechanism (Cameron & Fowler 1971) may occur in the merger scenario (Longland et al. 2012; Lauer et al. 2019). Recent work also indicates that the large IR shells seen around RCB stars are not fossil planetary nebula shells which would point toward the final flash (Montiel et al. 2015, 2018). Overall, it is not unreasonable to envisage that the fraction of RCB stars formed by the final-flash scenario could be at level of only  $\sim 10\%$ . In that case, the agreement between our estimate of the total number of Galactic RCB stars and the number predicted to exist via the double-degenerate channel is still holding. Of course, the fraction of RCB stars formed by either channel will need further observations to confirm this general impression.

## 7. Summary

From the  $\sim 563$  million objects catalogued by the WISE All-Sky survey, we selected 2356 targets of interest that present similar near- and mid-IR colours and brightness to typical known RCB stars. We used the 101 known Galactic and Magellanic RCB stars as a reference sample and found that 85% of them passed all our selection criteria. This emphasises the high detection efficiency of our selection criteria within  $\sim 50$  kpc from the sun. This list of 2356 ToI supersedes the one created using the WISE Preliminary data release (Tisserand 2012). Further studies and spectroscopic follow-up are now needed to discover the true nature of each of them.

All 2356 targets of interest have been classified into five different groups to prioritise further spectroscopy follow-up. We have respectively 375, 463, 1005, 298 and 215 targets reported in Groups #1 to #5, in order of priority. Group #1 is expected to result in the highest proportion of new RCB stars discovered. The majority of known RCB stars would have been reported in Group #1, typical RCB stars with a photospheric temperature between  $4000 < T_{\text{phot}} < 8000$  K and with a thick circumstellar

shell of temperature between  $500 < T_{\text{shell}} < 900$  K. Group #2 corresponds to similar RCB stars but with a higher  $J - K > 3.5$  mag colour index indicating high extinction. This Group is contaminated by highly enshrouded AGB stars, but can also reveal uncommon highly enshrouded RCB stars, such as MSX-SMC-014 and EROS2-SMC-RCB-4.

Using RCB SED models, we found that our photometric selection has a low detection efficiency with RCB stars that possess one of these three characteristics: (1) a cold circumstellar shell ( $T_{\text{shell}} < 400$  K), (2) a very thin shell as their SEDs would appear similar to classical F or G stars, or (3) a second colder and thicker shell, like the one seen around MV Sgr (Tisserand 2012). Furthermore, we are less efficient at detecting RCB stars whose 2MASS epoch coincides with a large decline in brightness. As reported in selection cut #3, it particularly affects RCB stars that possess a warm shell or those with high extinction in any combination of interstellar and circumstellar dust. Finally, we note that we expect to be less sensitive in the sky area  $-2 < b < 2$  deg and  $-60 < l < 60$  deg, where the interstellar extinction is higher than  $A_K > 3$  mag. We report some bright targets in that region, but further work with datasets obtained with surveys of higher spatial resolution, such as the VISTA/VVV and *Spitzer*/GLIMPSE surveys, should help us to probe this crowded part of the sky more efficiently.

We have obtained spectra for nearly 500 ToI, and thanks to the light curves produced by OGLE, ASAS, and other surveys, we can give a definite classification to about a third of the 2356 ToI. All spectra, light curves, and charts accumulated for each of them are available online<sup>6</sup>. We encourage all observers to report their own observations and help to keep this database up to date.

Spectroscopic selection criteria were defined using known RCB star spectra and hydrogen-deficient stellar atmosphere models to reveal new RCB stars with a range of temperature and abundances. The special scenario of dust obscuration events was

<sup>6</sup> <http://rcb.iap.fr/trackingrcb/>

also considered. We found 45 new RCB stars and also confirmed the long-lasting candidate KDM 5651 as an RCB star. Now, 117 Galactic and 30 Magellanic RCB stars are known. We also added a list of 14 strong Cold RCB star candidates for which further follow-up, particularly at a brighter phase, is needed. We strongly suspect them to be RCB stars as we have strong indications that their respective spectra were taken during a decline phase. These candidates are also mostly located near the Galactic plane, where the interstellar extinction is higher, making them more difficult to observe.

Light curve information is useful to identify other classes of variable stars, like Miras, but is not sufficient to identify an RCB star. Only the accumulation of evidence, and especially spectra taken in the bright phase, can confirm new RCB stars. For example, we have shown in the present work that the star OGLE-GC-RCB-2 is not an RCB star. It was wrongly reported as such by Tisserand et al. (2011) based only on its light curve, but the spectrum once obtained shows it to be an RV Tauri star. Indeed RV Tauri type stars share the same photometric colours as RCB stars in the optical and IR, but can also display fast and large photometric declines.

This work is the most systematic survey of RCB stars over the whole sky ever undertaken. Considering that RCB stars account for about 85% of all stars belonging to the larger class of HdC stars, we have estimated the total number of HdC stars located in the Milky Way to be no more than 500, with the most realistic range being between 300 and 500. This estimate is consistent with the total number of Magellanic RCB stars extrapolated to the mass of the Milky Way which corresponds to a total of about 550. Furthermore, this estimate matches well with theoretical predictions made from population synthesis. Indeed, between 100 and 500 RCB stars, formed from white-dwarf binary mergers are predicted to exist nowadays. As RCB stars could also be formed via the final helium shell flash mechanism, the challenge is now to measure the fraction of existing RCB stars formed via the double-degenerate and final-flash channels.

Overall, we found 30 Cold ( $T_{\text{eff}} < 6800$  K), 14 Warm ( $T_{\text{eff}} > 6800$  K) and one Hot ( $T_{\text{eff}} > 15\,000$  K) RCB stars, reaching totals of 97, 45 and 5 respectively for known Cold, Warm, and Hot RCB stars. The ratios between these temperature regimes could tell us about the relative time spent during the RCB star evolution across the HR diagram while its atmosphere contracts and heats (see Saio & Jeffery 2002, Figs. 2 and 3, and Lauer et al. 2019). This effect is expected to exist in both double-degenerate and final-flash formation scenarios. In the double-degenerate scenario, the situation is complex as there should exist a range of RCB stars masses, thus their  $T_{\text{eff}}$  and their evolution are highly governed by their respective original CO core mass and the envelope mass after accretion (Saio & Jeffery 2002; Lauer et al. 2019).

In the future, we will have to focus our observational efforts along the Galactic disc using northern telescopes. Also, to probe within the Galactic Centre area, and to examine fainter targets such as the ToI that compose priority group #4 (i.e. to find and understand RCB stars that are highly enshrouded), we will have to use 4m class telescopes. Then, for these highly obscured RCB stars, the main difficulties will come from the lack of crucial information in the visible such as the  $^{13}\text{C}$  absorption lines, knowledge of the hydrogen abundance from the CH bands or the  $\text{H}_\alpha$  line, but also the interesting  $\text{C}_2$  band-heads between 6000 and 6200 Å. Only the redder CN band-heads and the Ca II IR triplet will remain generally observable. The large dataset of *Gaia* will in the coming years be very useful to disentangle RCB stars from other variable stars. The infrared (0.9 to 2.0  $\mu\text{m}$ ) spectroscopic

all-sky survey planned by the EUCLID mission (Maciaszek et al. 2016) will also be a great help.

*Acknowledgements.* PT personally thank Tony Martin-Jones for his highly careful readings and comments. This research was conducted by the Australian Research Council Centre of Excellence for All-sky Astrophysics (CAASTRO), through project number CE110001020, and we acknowledge also financial support from “Programme National de Physique Stellaire” (PNPS) of CNRS/INSU, France. PT thanks the MARCS team in Uppsala (Sweden) for kindly providing a grid of hydrogen-deficient stellar models and the french embassy in Sweden for allowing a collaborative visit funded by the program TOR. We also thanks the team located at Siding Spring Observatory that keeps the 2.3 m telescope and its instruments is good shape, as well as the engineer, computer and technician teams located at Mount Stromlo Observatory that have facilitate the observations for the past 10 years. This research has made use of the SIMBAD database, operated at CDS, Strasbourg, France. This publication makes use of data products from the Wide-field Infrared Survey Explorer, which is a joint project of the University of California, Los Angeles, and the Jet Propulsion Laboratory/California Institute of Technology, funded by the National Aeronautics and Space Administration. This publication also makes use of data products from the Two Micron All Sky Survey, which is a joint project of the University of Massachusetts and the Infrared Processing and Analysis Centre, California Institute of Technology, funded by the National Aeronautics and Space Administration and the National Science Foundation. Finally, we heartily thank the OGLE team that have provided light curves for many of our candidates. The OGLE project has received funding from the National Science Centre, Poland, grant MAESTRO 2014/14/A/ST9/00121 to A.U.

## References

- Alcock, C., Allsman, R. A., Alves, D. R., et al. 2001, *ApJ*, 554, 298  
 Alvarez, R., & Plez, B. 1998, *A&A*, 330, 1109  
 Asplund, M., Gustafsson, B., Lambert, D. L., & Rao, N. K. 2000, *A&A*, 353, 287  
 Bell, R. A., Eriksson, K., Gustafsson, B., & Nordlund, A. 1976, *A&AS*, 23, 37  
 Bessell, M. S., & Wood, P. R. 1983, *MNRAS*, 202, 31P  
 Bhowmick, A., Pandey, G., Joshi, V., & Ashok, N. M. 2018, *ApJ*, 854, 140  
 Cameron, A. G. W., & Fowler, W. A. 1971, *ApJ*, 164, 111  
 Churchwell, E., Babler, B. L., Meade, M. R., et al. 2009, *PASP*, 121, 213  
 Clayton, G. C. 1996, *PASP*, 108, 225  
 Clayton, G. C. 2012, *J. Am. Assoc. Variable Star Obs.*, 40, 539  
 Clayton, G. C., Geballe, T. R., Herwig, F., Fryer, C., & Asplund, M. 2007, *ApJ*, 662, 1220  
 Clayton, G. C., Sugerman, B. E. K., Stanford, S. A., et al. 2011, *ApJ*, 743, 44  
 Clayton, G. C., Geballe, T. R., & Zhang, W. 2013, *AJ*, 146, 23  
 Cottrell, P. L., Lawson, W. A., & Buchhorn, M. 1990, *MNRAS*, 244, 149  
 Cutri, R. M., Skrutskie, M. F., van Dyk, S., et al. 2003, *VizieR Online Data Catalog*: II/246  
 Cutri, R. M., Wright, E. L., Conrow, T., et al. 2011, *Explanatory Supplement to the WISE Preliminary Data Release Products*, Tech. rep.  
 Cutri, R. M., Wright, E. L., Conrow, T., et al. 2012, *Explanatory Supplement to the WISE All-Sky Data Release Products*, Tech. rep.  
 Dahari, O., & Osterbrock, D. E. 1984, *ApJ*, 277, 648  
 De Marco, O., Clayton, G. C., Herwig, F., et al. 2002, *AJ*, 123, 3387  
 Dopita, M., Hart, J., McGregor, P., et al. 2007, *Ap&SS*, 310, 255  
 Drake, A. J., Djorgovski, S. G., Mahabal, A., et al. 2009, *ApJ*, 696, 870  
 García-Hernández, D. A., Lambert, D. L., Kameswara Rao, N., Hinkle, K. H., & Eriksson, K. 2010, *ApJ*, 714, 144  
 García-Hernández, D. A., Rao, N. K., & Lambert, D. L. 2011, *ApJ*, 739, 37  
 Gezer, I., Van Winckel, H., Bozkurt, Z., et al. 2015, *MNRAS*, 453, 133  
 Gustafsson, B., Bell, R. A., Eriksson, K., & Nordlund, A. 1975, *A&A*, 42, 407  
 Gustafsson, B., Edvardsson, B., Eriksson, K., et al. 2008, *A&A*, 486, 951  
 Hackstein, M., Fein, C., Haas, M., et al. 2015, *Astron. Nachr.*, 336, 590  
 Hartwick, F. D. A., & Cowley, A. P. 1988, *ApJ*, 334, 135  
 Hema, B. P., Pandey, G., & Lambert, D. L. 2012, *ApJ*, 747, 102  
 Houk, N. 1967, *Inf. Bull. Variable Stars*, 228, 1  
 Iben, I. J., Tutukov, A. V., & Yungelson, L. R. 1996, *ApJ*, 456, 750  
 Jayasinghe, T., Stanek, K. Z., Kochanek, C. S., et al. 2017, *ATel*, 11017  
 Jayasinghe, T., Kochanek, C. S., Stanek, K. Z., et al. 2018, *MNRAS*, 477, 3145  
 Jeffery, C. S. 2008a, in *Hydrogen-Deficient Stars*, eds. A. Werner, & T. Rauch, *ASP Conf. Ser.*, 391, 3  
 Jeffery, C. S. 2008b, in *Hydrogen-Deficient Stars*, eds. A. Werner, & T. Rauch, *ASP Conf. Ser.*, 391, 53  
 Jeffery, C. S., Karakas, A. I., & Saio, H. 2011, *MNRAS*, 414, 3599  
 Kamath, D., Wood, P. R., & Van Winckel, H. 2014, *MNRAS*, 439, 2211  
 Kamath, D., Wood, P. R., & Van Winckel, H. 2015, *MNRAS*, 454, 1468

- Kameswara-Rao, N., & Lambert, D. L. 1993, *MNRAS*, **263**, L27
- Kameswara Rao, N., Reddy, B. E., & Lambert, D. L. 2004, *MNRAS*, **355**, 855
- Kameswara Rao, N., Lambert, D. L., & Shetrone, M. D. 2006, *MNRAS*, **370**, 941
- Karakas, A. I., Ruitter, A. J., & Hampel, M. 2015, *ApJ*, **809**, 184
- Kilkenny, D., & Marang, F. 1989, *MNRAS*, **238**, 1
- Kraemer, K. E., Sloan, G. C., Wood, P. R., Price, S. D., & Egan, M. P. 2005, *ApJ*, **631**, L147
- Lauer, A., Chatzopoulos, E., Clayton, G. C., Frank, J., & Marcelllo, D. C. 2019, *MNRAS*, **488**, 438
- Lawson, W. A. 1992, *MNRAS*, **258**, 33P
- Lawson, W. A., & Cottrell, P. L. 1989, *MNRAS*, **240**, 689
- Lawson, W. A., & Cottrell, P. L. 1997, *MNRAS*, **285**, 266
- Lee, C.-H. 2015, *A&A*, **575**, A2
- Leuenhagen, U., Heber, U., & Jeffery, C. S. 1994, *A&AS*, **103**, 445
- Longland, R., Lorén-Aguilar, P., José, J., García-Berro, E., & Althaus, L. G. 2012, *A&A*, **542**, A117
- Maciaszek, T., Ealet, A., Jahnke, K., et al. 2016, in *Space Telescopes and Instrumentation 2016: Optical, Infrared, and Millimeter Wave*, Proc. SPIE, 9904, 99040T
- Mainzer, A., Bauer, J., Grav, T., et al. 2011, *ApJ*, **731**, 53
- Matsuura, M., Bernard-Salas, J., Lloyd Evans, T., et al. 2014, *MNRAS*, **439**, 1472
- McNaught, R. 1986, *IAU Circ.*, 4245
- Menon, A., Herwig, F., Denissenkov, P. A., et al. 2013, *ApJ*, **772**, 59
- Minniti, D., Lucas, P. W., Emerson, J. P., et al. 2010, *New A.*, **15**, 433
- Montiel, E. J., Clayton, G. C., Marcelllo, D. C., & Lockman, F. J. 2015, *AJ*, **150**, 14
- Montiel, E. J., Clayton, G. C., Sugerma, B. E. K., et al. 2018, *AJ*, **156**, 148
- Morgan, D. H., & Hatzidimitriou, D. 1995, *A&AS*, **113**, 539
- Morgan, D. H., Hatzidimitriou, D., Cannon, R. D., & Croke, B. F. W. 2003, *MNRAS*, **344**, 325
- Nelemans, G., Yungelson, L. R., Portegies Zwart, S. F., & Verbunt, F. 2001, *A&A*, **365**, 491
- Nikzat, F., & Catelan, M. 2016, *Inf. Bull. Variable Stars*, **6190**, 1
- Oostrum, L. C., Ochsendorf, B. B., Kaper, L., & Tielens, A. G. G. M. 2018, *A&A*, **610**, L6
- Pandey, G., Lambert, D. L., & Rao, N. K. 2008, *ApJ*, **674**, 1068
- Plez, B. 2008, *Phys. Scr. Vol. T*, **133**, 014003
- Plez, B. 2012, Astrophysics Source Code Library [record ascl:1205.004]
- Pojmanski, G. 1997, *Acta Astron.*, **47**, 467
- Rao, N. K., & Lambert, D. L. 2008, *MNRAS*, **384**, 477
- Rebeiro, E., Azzopardi, M., & Westerlund, B. E. 1993, *A&AS*, **97**, 603
- Renzini, A. 1990, in 11: Confrontation Between Stellar Pulsation and Evolution, eds. C. Cacciari, & G. Clementini, *ASP Conf. Ser.*, 549
- Richer, H. B. 1971, *ApJ*, **167**, 521
- Ruffle, P. M. E., Kemper, F., Jones, O. C., et al. 2015, *MNRAS*, **451**, 3504
- Ruitter, A. J., Belczynski, K., & Fryer, C. 2009, *ApJ*, **699**, 2026
- Ryabchikova, T., Piskunov, N., Kurucz, R. L., et al. 2015, *Phys. Scr.*, **90**, 054005
- Saio, H., & Jeffery, C. S. 2002, *MNRAS*, **333**, 121
- Schaefer, B. E. 2016, *MNRAS*, **460**, 1233
- Schlafly, E. F., & Finkbeiner, D. P. 2011, *ApJ*, **737**, 103
- Shappee, B., Prieto, J., Stanek, K. Z., et al. 2014, *Astron. Soc. Meeting Abstr.*, **223**, 03
- Sharp, R., Saunders, W., Smith, G., et al. 2006, *SPIE*, **6269**, 62690G
- Shields, J. V., Jayasinghe, T., Stanek, K. Z., et al. 2019, *MNRAS*, **483**, 4470
- Skrutskie, M. F., Cutri, R. M., Stiening, R., et al. 2006, *AJ*, **131**, 1163
- Soszyński, I., Udalski, A., Szymański, M. K., et al. 2009, *Acta Astron.*, **59**, 335
- Spite, F., & Spite, M. 1979, *A&A*, **80**, 61
- Staff, J. E., Menon, A., Herwig, F., et al. 2012, *ApJ*, **757**, 76
- Tisserand, P. 2012, *A&A*, **539**, A51
- Tisserand, P., Marquette, J. B., Beaulieu, J. P., et al. 2004, *A&A*, **424**, 245
- Tisserand, P., Marquette, J. B., Wood, P. R., et al. 2008, *A&A*, **481**, 673
- Tisserand, P., Wood, P. R., Marquette, J. B., et al. 2009, *A&A*, **501**, 985
- Tisserand, P., Wyrzykowski, L., Wood, P. R., et al. 2011, *A&A*, **529**, A118
- Tisserand, P., Clayton, G. C., Welch, D. L., et al. 2013, *A&A*, **551**, A77
- Udalski, A. 2003, *Acta Astron.*, **53**, 291
- Woods, P. M., Oliveira, J. M., Kemper, F., et al. 2011, *MNRAS*, **411**, 1597
- Wright, E. L., Eisenhardt, P. R. M., Mainzer, A. K., et al. 2010, *AJ*, **140**, 1868
- Zaniewski, A., Clayton, G. C., Welch, D. L., et al. 2005, *AJ*, **130**, 2293
- Zhang, X., Jeffery, C. S., Chen, X., & Han, Z. 2014, *MNRAS*, **445**, 660

## Appendix A: Previously known RCB stars and strong RCB stars candidates

Table A.1. WISE All-Sky magnitudes and errors for all previously known RCB stars and strong RCB candidates.

Name	[3.4]	$\sigma_{[3.4]}$	[4.6]	$\sigma_{[4.6]}$	[12]	$\sigma_{[12]}$	[22]	$\sigma_{[22]}$
Galactic RCB stars								
XX Cam	5.395	0.064	5.10 <sup>(a)</sup>	0.032	3.453	0.015	2.837	0.020
SU Tau	4.829	0.078	3.56 <sup>(a)</sup>	0.1	1.526	0.011	0.984	0.012
UX Ant	9.799	0.022	8.470	0.020	6.375	0.018	5.681	0.040
UW Cen	5.360	0.053	3.78 <sup>(a)</sup>	0.1	1.490	0.007	0.623	0.011
Y Mus	8.112	0.023	7.844	0.021	5.879	0.015	4.621	0.032
DY Cen	10.427	0.022	9.173	0.021	4.132	0.013	2.340	0.009
V854 Cen	3.187	0.144	2.49 <sup>(a)</sup>	0.1	0.533	0.007	0.381	0.008
Z Umi	5.994	0.051	5.02 <sup>(a)</sup>	0.037	3.455	0.012	2.894	0.016
S Aps	6.057	0.053	5.67 <sup>(a)</sup>	0.028	3.780	0.014	2.815	0.018
R CrB	3.455	0.140	2.37 <sup>(a)</sup>	0.1	-0.498	0.020	-0.813	0.008
RT Nor	5.838	0.052	4.48 <sup>(a)</sup>	0.048	2.901	0.011	2.583	0.018
RZ Nor	6.686	0.031	5.12 <sup>(a)</sup>	0.036	2.879	0.015	2.045	0.018
V517 Oph	4.933	0.069	3.71 <sup>(a)</sup>	0.1	2.096	0.010	1.577	0.014
V1783 Sgr	6.118	0.039	5.34 <sup>(a)</sup>	0.027	3.169	0.014	2.297	0.018
WX CrA	6.227	0.039	5.34 <sup>(a)</sup>	0.033	3.842	0.014	3.225	0.024
V739 Sgr	6.441	0.036	5.49 <sup>(a)</sup>	0.029	3.854	0.015	3.191	0.021
V3795 Sgr	7.122	0.027	5.60 <sup>(a)</sup>	0.024	3.081	0.013	2.375	0.017
VZ Sgr	7.392	0.026	6.458	0.019	4.962	0.015	4.249	0.027
RS Tel	7.068	0.030	5.79 <sup>(a)</sup>	0.028	3.705	0.014	3.021	0.021
GU Sgr	5.951	0.056	4.71 <sup>(a)</sup>	0.037	3.053	0.011	2.590	0.016
V348 Sgr	5.249	0.043	3.75 <sup>(a)</sup>	0.1	2.046	0.012	1.342	0.017
MV Sgr	8.124	0.022	7.401	0.020	4.725	0.014	2.193	0.016
FH Sct	6.062	0.043	5.11 <sup>(a)</sup>	0.037	3.625	0.015	2.977	0.022
V CrA	5.790	0.049	4.39 <sup>(a)</sup>	0.1	2.310	0.010	1.566	0.014
SV Sge	5.588	0.060	5.30 <sup>(a)</sup>	0.035	3.352	0.012	2.153	0.016
V1157 Sgr	6.288	0.043	4.94 <sup>(a)</sup>	0.045	null	null	null	null
RY Sgr	3.036	0.156	2.27 <sup>(a)</sup>	0.193	-0.144	0.029	-0.561	0.018
V482 Cyg	5.835	0.055	5.23 <sup>(a)</sup>	0.033	4.009	0.014	3.489	0.020
U Aqr	7.681	0.025	6.712	0.020	4.386	0.015	3.377	0.019
UV Cas	6.734	0.036	6.20 <sup>(a)</sup>	0.022	4.218	0.015	3.066	0.022
ES Aql	5.939	0.050	5.00 <sup>(a)</sup>	0.038	3.368	0.013	2.800	0.018
V2552 Oph	7.349	0.026	6.25 <sup>(a)</sup>	0.021	4.787	0.015	4.255	0.025
V4017 Sgr	7.332	0.028	6.35 <sup>(a)</sup>	0.020	4.691	0.010	3.925	0.020
V532 Oph	6.834	0.028	5.87 <sup>(a)</sup>	0.024	4.221	0.015	3.611	0.023
NSV11154	8.083	0.023	7.099	0.020	5.183	0.015	4.351	0.025
AO Her	5.436	0.065	4.10 <sup>(a)</sup>	0.1	2.371	0.007	1.797	0.009
ASAS-RCB-1	5.915	0.041	5.51 <sup>(a)</sup>	0.029	3.703	0.014	2.423	0.022
ASAS-RCB-2	4.412	0.084	3.39 <sup>(a)</sup>	0.1	1.755	0.012	1.140	0.011
ASAS-RCB-3	6.277	0.039	5.22 <sup>(a)</sup>	0.033	3.774	0.014	3.261	0.018
ASAS-RCB-4	6.669	0.040	5.65 <sup>(a)</sup>	0.031	4.172	0.014	3.723	0.020
ASAS-RCB-5	5.944	0.043	4.73 <sup>(a)</sup>	0.038	3.293	0.011	2.696	0.021
ASAS-RCB-6	9.380	0.024	8.337	0.020	5.964	0.015	4.922	0.026
ASAS-RCB-7	7.120	0.030	5.92 <sup>(a)</sup>	0.027	4.137	0.015	3.382	0.022
ASAS-RCB-8	9.481	0.023	9.277	0.021	7.669	0.028	6.718	0.163
ASAS-RCB-9	5.203	0.059	3.96 <sup>(a)</sup>	0.1	2.199	0.013	1.530	0.019
ASAS-RCB-10	6.933	0.030	5.81 <sup>(a)</sup>	0.027	4.329	0.016	3.931	0.023
ASAS-RCB-11	6.384	0.041	5.51 <sup>(a)</sup>	0.027	4.210	0.015	3.675	0.023
ASAS-RCB-12	5.573	0.053	4.71 <sup>(a)</sup>	0.040	3.153	0.013	2.469	0.019
ASAS-RCB-13	4.375	0.082	2.83 <sup>(a)</sup>	0.1	0.677	0.016	0.175	0.008
ASAS-RCB-14	6.158	0.047	4.93 <sup>(a)</sup>	0.038	3.166	0.013	2.511	0.020

**Notes.** <sup>(a)</sup>[4.6] original magnitude was corrected for photometric bias observed at high saturation level (see Sect. 4). <sup>(r1)</sup>Listed in Tisserand et al. (2011). <sup>(r2)</sup>Featureless mid-IR spectrum presented by Matsuura et al. (2014) and listed in Soszyński et al. (2009) as OGLE LMC-RCB-21. <sup>(r3)</sup>Featureless mid-IR spectrum presented by Woods et al. (2011). <sup>(r4)</sup>Listed in Morgan et al. (2003) as a strong RCB candidate. <sup>(r5)</sup>Listed in Tisserand et al. (2009) due to their interesting light curves.

Table A.1. continued.

Name	[3.4]	$\sigma_{[3.4]}$	[4.6]	$\sigma_{[4.6]}$	[12]	$\sigma_{[12]}$	[22]	$\sigma_{[22]}$
ASAS-RCB-15	6.544	0.036	5.45 <sup>(a)</sup>	0.032	3.844	0.014	3.207	0.027
ASAS-RCB-16	6.794	0.035	5.92 <sup>(a)</sup>	0.023	4.445	0.015	3.979	0.022
ASAS-RCB-17	7.656	0.023	6.35 <sup>(a)</sup>	0.022	4.391	0.014	3.667	0.022
ASAS-RCB-18	6.512	0.036	5.51 <sup>(a)</sup>	0.030	3.843	0.015	3.056	0.018
ASAS-RCB-19	6.122	0.042	5.12 <sup>(a)</sup>	0.038	3.327	0.011	2.641	0.020
ASAS-RCB-20	5.648	0.054	4.33 <sup>(a)</sup>	0.1	2.203	0.008	1.309	0.014
ASAS-RCB-21	4.857	0.058	3.38 <sup>(a)</sup>	0.1	1.323	0.011	0.592	0.014
IRAS1813.5-2419	6.469	0.033	5.77 <sup>(a)</sup>	0.025	4.254	0.014	3.498	0.023
ASAS-RCB-18	6.512	0.036	5.51 <sup>(a)</sup>	0.030	3.843	0.015	3.056	0.018
ASAS-RCB-19	6.122	0.042	5.12 <sup>(a)</sup>	0.038	3.327	0.011	2.641	0.020
ASAS-RCB-20	5.648	0.054	4.33 <sup>(a)</sup>	0.1	2.203	0.008	1.309	0.014
ASAS-RCB-21	4.857	0.058	3.38 <sup>(a)</sup>	0.1	1.323	0.011	0.592	0.014
IRAS1813.5-2419	6.469	0.033	5.77 <sup>(a)</sup>	0.025	4.254	0.014	3.498	0.023
V391 Sct	8.069	0.023	7.119	0.021	5.421	0.016	4.787	0.031
MACHO 135.27132.51	8.312	0.023	7.022	0.021	5.067	0.014	4.236	0.025
MACHO 301.45783.9	8.515	0.024	7.167	0.020	5.382	0.014	4.544	0.025
MACHO 308.38099.66	7.639	0.022	6.509	0.020	4.850	0.014	4.016	0.024
MACHO 401.48170.2237	5.898	0.042	4.82 <sup>(a)</sup>	0.042	3.440	0.015	2.806	0.023
EROS2-CG-RCB-1	6.628	0.036	4.94 <sup>(a)</sup>	0.027	3.244	0.013	2.325	0.017
EROS2-CG-RCB-3	5.737	0.049	4.44 <sup>(a)</sup>	0.055	3.148	0.012	2.533	0.016
EROS2-CG-RCB-4	6.423	0.034	5.34 <sup>(a)</sup>	0.033	3.649	0.010	2.897	0.022
EROS2-CG-RCB-5	6.233	0.031	5.08 <sup>(a)</sup>	0.022	3.817	0.009	3.080	0.019
EROS2-CG-RCB-6	7.104	0.029	6.00 <sup>(a)</sup>	0.023	4.350	0.017	3.641	0.031
EROS2-CG-RCB-7	7.156	0.030	6.11 <sup>(a)</sup>	0.021	4.621	0.014	3.911	0.026
EROS2-CG-RCB-8	6.999	0.029	5.88 <sup>(a)</sup>	0.025	4.224	0.015	3.555	0.030
EROS2-CG-RCB-9	7.221	0.026	5.58 <sup>(a)</sup>	0.026	3.464	0.012	2.613	0.023
EROS2-CG-RCB-10	6.747	0.034	4.82 <sup>(a)</sup>	0.039	2.612	0.011	1.914	0.021
EROS2-CG-RCB-11	6.513	0.029	5.61 <sup>(a)</sup>	0.020	4.152	0.009	3.476	0.021
EROS2-CG-RCB-12	8.044	0.023	7.385	0.019	6.485	0.013	6.254	0.063
EROS2-CG-RCB-13	6.815	0.032	5.67 <sup>(a)</sup>	0.026	4.017	0.014	3.345	0.023
EROS2-CG-RCB-14	6.404	0.031	5.05 <sup>(a)</sup>	0.032	3.337	0.010	2.640	0.015
OGLE-GC-RCB-1	6.683	0.035	5.72 <sup>(a)</sup>	0.024	4.061	0.014	3.347	0.020
Magellanic RCB stars								
HV 5637	11.780	0.024	11.101	0.020	8.319	0.017	7.422	0.055
W Men	9.998	0.022	9.138	0.020	7.966	0.016	7.577	0.078
HV 12842	10.568	0.023	9.131	0.020	7.036	0.015	6.303	0.029
MACHO-11.8632.2507	10.043	0.023	8.761	0.020	6.403	0.014	4.178	0.019
MACHO-81.8394.1358	10.807	0.023	9.658	0.020	7.891	0.019	7.400	0.067
MACHO-6.6575.13	9.898	0.021	8.355	0.019	5.922	0.012	4.926	0.019
MACHO-6.6696.60	10.427	0.023	9.141	0.020	6.815	0.016	5.707	0.025
MACHO-12.10803.56	10.269	0.023	9.356	0.020	7.738	0.015	6.954	0.034
MACHO-16.5641.22	10.030	0.023	9.042	0.021	7.304	0.016	6.779	0.049
MACHO-18.3325.148	10.475	0.023	9.205	0.020	7.090	0.015	6.467	0.058
MACHO-79.5743.15	9.993	0.023	8.606	0.022	6.785	0.016	6.285	0.042
MACHO-80.6956.207	10.253	0.024	9.136	0.020	7.481	0.019	6.834	0.039
MACHO-80.7559.28	9.695	0.022	8.786	0.020	6.959	0.015	5.859	0.030
EROS2-LMC-RCB-1	10.499	0.022	9.211	0.019	7.453	0.018	6.924	0.061
EROS2-LMC-RCB-2	10.918	0.024	9.741	0.020	7.462	0.019	6.933	0.081
EROS2-LMC-RCB-3	11.574	0.023	10.601	0.021	7.803	0.020	7.091	0.100

Table A.1. continued.

Name	[3.4]	$\sigma_{[3.4]}$	[4.6]	$\sigma_{[4.6]}$	[12]	$\sigma_{[12]}$	[22]	$\sigma_{[22]}$
EROS2-LMC-RCB-4	9.981	0.023	8.541	0.020	6.671	0.015	6.137	0.031
EROS2-LMC-RCB-5	11.842	0.023	11.362	0.021	8.658	0.018	7.395	0.062
EROS2-LMC-RCB-6	10.591	0.023	9.073	0.021	6.885	0.015	6.085	0.034
ASASJ050232-7218.9	11.116	0.023	9.279	0.019	6.473	0.015	5.747	0.031
EROS2-SMC-RCB-1	11.000	0.024	9.775	0.021	7.957	0.018	7.494	0.098
EROS2-SMC-RCB-2	11.148	0.023	10.119	0.021	8.133	0.018	7.246	0.083
EROS2-SMC-RCB-3	9.807	0.023	8.458	0.021	6.552	0.015	5.874	0.034
MSX-SMC-014	10.269	0.024	8.690	0.020	6.365	0.014	5.378	0.028
Strong RCB stars candidates (look at discussions and at possible update in their status in Sect. 5)								
OGLE-GC-RCB-Cand-1 <sup>(r1)</sup>	7.011	0.030	6.07 <sup>(a)</sup>	0.023	4.057	0.013	2.405	0.018
OGLE-GC-RCB-Cand-2 <sup>(r1)</sup>	7.792	0.025	7.048	0.022	5.463	0.015	4.635	0.033
GLIMPSE-RCB-Cand-1 <sup>(r1)</sup>	6.822	0.029	5.57 <sup>(a)</sup>	0.025	3.992	0.013	3.463	0.018
GLIMPSE-RCB-Cand-2 <sup>(r1)</sup>	5.689	0.059	4.48 <sup>(a)</sup>	0.051	3.098	0.012	2.583	0.019
MSX-LMC-1795 <sup>(r2)</sup>	10.03	0.023	8.577	0.02	6.414	0.016	5.317	0.031
[RP2006] 1631 <sup>(r3)</sup>	10.738	0.023	9.644	0.020	7.707	0.017	6.371	0.045
KDM 5651 <sup>(r4)</sup>	11.419	0.023	10.389	0.021	8.960	0.027	9.690	0.392
EROS2-LMC-RCB-7 <sup>(r5)</sup>	9.577	0.022	7.965	0.020	5.504	0.014	4.373	0.021
EROS2-LMC-RCB-8 <sup>(r5)</sup>	9.737	0.023	8.701	0.020	7.290	0.015	6.976	0.055
EROS2-SMC-RCB-4 <sup>(r5)</sup>	11.538	0.023	9.519	0.019	6.697	0.014	5.585	0.028

**Appendix B: New Galactic and Magellanic RCB stars discovered and the new strong RCB stars candidates****Table B.1.** Summary on spectroscopic temperature group and light curves variation found for all newly confirmed Galactic and Magellanic RCB stars and of the new strong RCB stars candidates.

WISE All-Sky designation	WISE-ToI Id	Galactic coordinates		Temperature group	Spectroscopic instrument	Light curve, survey and largest variations observed
		l (deg)	b (deg)			
New Galactic RCB stars						
J110008.77-600303.6	76	289.45754	-0.12330	Cold	2.3 m/WiFeS	
J132354.47-673720.8	90	306.02499	-4.94583	Cold	2.3 m/WiFeS	
J150104.50-563325.1	105	320.12182	1.92522	Cold	2.3 m/WiFeS	Bochum: 1.0 mag variation
J160205.48-552741.6	121	327.72638	-2.05059	Cold	2.3 m/WiFeS	Bochum: 0.4 mag variation
J161156.23-575527.1	124	327.07187	-4.78229	Cold	2.3 m/WiFeS	ASAS-SN: 2.5 mag drop <sup>(#)</sup>
J163450.35-380218.5	130	343.92434	6.46016	Cold	2.3 m/WiFeS	
J164704.67-470817.8	139	338.56953	-1.23860	Warm	2.3 m/WiFeS	Bochum: 3.0 mag variation
J170343.87-385126.6	148	346.92365	1.59123	Cold	2.3 m/WiFeS	
J171815.36-341339.9	161	352.38354	1.97860	Cold	2.3 m/WiFeS	
J171908.50-435044.6	1220	344.60551	-3.68706	Cold	2.3 m/WiFeS	
J172447.52-290418.6	169	357.42448	3.75908	Warm	2.3 m/WiFeS	
J172553.80-312421.1	171	355.62021	2.25628	Warm	2.3 m/WiFeS	
J172951.80-101715.9 <sup>(r1)</sup>	174	14.05807	12.92716	Warm	2.3 m/WiFeS	CRTS: no variation
J173202.75-432906.1	1222	346.20875	-5.42525	Cold	2.3 m/WiFeS	
J173553.02-364104.3	177	352.34341	-2.37032	Cold	2.3 m/WiFeS	
J173819.81-203632.1	1227	6.22662	5.78226	Cold	2.3 m/WiFeS	
J174111.80-281955.3	No Id	0.00465	1.14323	Warm	2.3 m/WiFeS	
J174119.57-250621.2	No Id	2.76109	2.82268	Warm	2.3 m/WiFeS	
J174138.87-161546.4	182	10.37103	7.38144	Cold	2.3 m/WiFeS	ASAS: 0.9 mag (oscillations?)
J174257.19-362052.1	184	353.38413	-3.39531	Cold	2.3 m/WiFeS	OGLE: 8.0 mag (4 drops)
J174328.50-375029.0	186	352.16205	-4.26413	Cold	2.3 m/WiFeS	OGLE: 4.0 mag (2 drops)
J174645.90-250314.1 <sup>(r2)</sup>	188	3.44972	1.80007	Warm	2.3 m/WiFeS	OGLE: 8.0 mag (2 drops)
J174851.29-330617.0	190	356.79067	-2.75043	Warm	2.3 m/WiFeS	
J175031.70-233945.7	191	5.08443	1.78184	Warm	2.3 m/WiFeS	OGLE: 1.2 mag (1 small drop)
J175107.12-242357.3	193	4.52017	1.28935	Warm	2.3 m/WiFeS	OGLE: no variation
J175521.75-281131.2	1241	1.73524	-1.45559	Cold	SOAR/Goodman	OGLE: 8.0 mag (5 drops)
J175558.51-164744.3	197	11.66355	4.15326	Warm	2.3 m/WiFeS	
J175749.76-075314.9	203	19.68570	8.14974	Cold	2.3 m/WiFeS	ASAS-SN: >1.8 mag <sup>(M)</sup> (1 drop)
J175749.98-182522.8 <sup>(r3)</sup>	204	10.47189	2.95757	Cold	2.3 m/WiFeS	
J180550.49-151301.7	209	14.21051	2.86870	Warm	2.3 m/WiFeS	ASAS: 1.0 mag variations
J181252.50-233304.4	2645	7.71430	-2.61157	Cold	2.3 m/WiFeS	OGLE: 1.6 mag (2 drops) ASAS-SN: >1.5 mag <sup>(M)</sup> (1 drop)
J181538.25-203845.7	220	10.57510	-1.78842	Cold	2.3 m/WiFeS	Pan-STARRS: >2.0 mag <sup>(M)</sup>
J182334.24-282957.1	1265	4.45107	-7.04796	Cold	2.3 m/WiFeS	
J182723.38-200830.1	1269	12.31294	-3.98522	Cold	2.3 m/WiFeS	
J182943.83-190246.2	231	13.54224	-3.97017	Cold	2.3 m/WiFeS	Bochum: 3.0 mag (1 drop)

**Notes.** <sup>(#)</sup>Reported as a likely RCB star based on a brightness drop observed by the ASAS-SN survey (Jayasinghe et al. 2017) and being flagged in Tisserand (2012) due to its IR colours characteristic. <sup>(##)</sup>A decline of  $\sim 1.6$  mag at JD $\sim 2458000$  days was observed by the monitoring survey ASAS-SN (Jayasinghe et al. 2018). <sup>(\*)</sup>Named GDS\_J1613117-503040 in the Bochum survey. <sup>(\*\*)</sup>Also known as KDM 5651 : previously known candidate RCB (Morgan et al. 2003) as reported by Stefan Hümmerich (light curve available on AAVSO variable star website). <sup>(r1)</sup>Also known as the variable star AC Ser. <sup>(r2)</sup>Listed as candidate RCB GLIMPSE-RCB-Cand-1 in Tisserand et al. (2011). <sup>(r3)</sup>Listed as candidate RCB GLIMPSE-RCB-Cand-2 in Tisserand et al. (2011). <sup>(r4)</sup>Also known as [MH95] 580, and *Gaia* 16aa, a *Gaia* Alert ATEL <http://www.astronomerstelegam.org/?read=8681>. <sup>(r5)</sup>Also known as RAW 658 in the SMC carbon stars catalogue from Rebeiro et al. (1993). <sup>(r6)</sup>Also known as MSX-LMC-1795 (Matsuura et al. 2014) and OGLE-LMC-RCB-21 (Soszyński et al. 2009). <sup>(r7)</sup>Also known as HV 12862 and KDM 6829. <sup>(r8)</sup>Also known as the variable star IZ Sgr. It was surprisingly classified as a Mira type star (M6 spectral type) by Houk (1967) after a spectroscopic follow-up. <sup>(M)</sup>Variations observed by Gabriel Murawski (priv. comm., 2019), light curves available on AAVSO variable star website.

Table B.1. continued.

WISE All-Sky designation	WISE-ToI Id	Galactic coordinates		Temperature group	Spectroscopic instrument	Light Curve, survey and largest variations observed
		l (deg)	b (deg)			
New Magellanic RCB stars						
J183649.54-113420.7	240	20.97746	-2.05850	Cold	2.3 m/WiFeS	Bochum: 5.0 mag (1 drop)
J184158.40-054819.2	249	26.68830	-0.54812	Cold	2.3 m/WiFeS	Bochum: 0.3 mag (1 small drop)
J184246.26-125414.7	250	20.45347	-3.95830	Cold	2.3 m/WiFeS	
J185525.52-025145.7	257	30.83712	-2.19132	Warm	2.3 m/WiFeS	Bochum: 0.2 mag and ASAS-SN: 1.6 mag <sup>(##)</sup> (1 drop)
J194218.38-203247.5	290	19.48694	-20.08972	Cold	2.3 m/WiFeS	CRTS: 8.0 mag (7 drops)
J005010.67-694357.7 <sup>(r4)</sup>	5003	303.09311	-47.39506	Warm	2.3 m/WiFeS	OGLE: 6.0 mag (2 drops)
J005113.58-731036.3 <sup>(r5)</sup>	5004	302.95316	-43.95139	Cold	2.3 m/WiFeS	OGLE: 7.0 mag (2 drops)
J053745.70-635330.8	6005	273.35887	-32.22225	Hot	2.3 m/WiFeS	OGLE: 5.0 mag (3 drops)
J054123.49-705801.8 <sup>(**)</sup>	No Id	281.60571	-31.22409	Cold	2.3 m/WiFeS	
J054221.91-690259.3 <sup>(r6)</sup>	5039	279.36499	-31.35237	Cold	2.3 m/WiFeS	OGLE: 6.0 mag (9 drops)
J055643.56-715510.7 <sup>(r7)</sup>	5042	282.57199	-29.91933	Cold/Warm	AAT/AAOmega 2.3 m/WiFeS	OGLE: no variation
New Galactic RCB candidates						
J161311.79-503040.2 <sup>(*)</sup>	No Id	332.29137	0.49038	n/a	not observed	Bochum: 3.0 mag (1 drop)
J164424.53-481205.1	136	337.46936	-1.58860	Cold	2.3 m/WiFeS	
J164433.19-423032.2	137	341.79607	2.11155	Cold	2.3 m/WiFeS	
J164440.88-421522.3	138	342.00320	2.25855	Cold	2.3 m/WiFeS	
J170738.27-431019.7	150	343.92942	-1.60193	Cold	2.3 m/WiFeS	
J172044.89-315031.7	164	354.64091	2.91539	Cold	2.3 m/WiFeS	
J173837.00-281734.5	181	359.73602	1.64518	Cold	2.3 m/WiFeS	Pan-STARRS: 5.9 mag <sup>(M)</sup> (1 drop)
J175136.80-220630.6	194	6.54934	2.36043	Cold	2.3 m/WiFeS	
J180313.12-251330.1	207	5.18282	-1.50019	Cold	2.3 m/WiFeS	
J181316.97-253135.1	218	6.02007	-3.63537	Cold	2.3 m/WiFeS	OGLE: 4.2 mag (1 drop) EROS2: 2.5 mag (1 drop)
J182010.96-193453.4	223	12.01864	-2.22483	Cold	2.3 m/WiFeS	
J182235.25-033213.2	225	26.47598	4.78381	Cold	2.3 m/WiFeS	
J183631.25-205915.1 <sup>(r8)</sup>	4117	12.53382	-6.27324	Cold	2.3 m/WiFeS	ASAS: 1.5 mag (2 drops)
J190309.89-302037.1	264	6.44446	-15.64277	Cold	2.3 m/WiFeS	
J191243.06+055313.1	274	40.59924	-2.02375	Cold	2.3 m/WiFeS	